EFDA–JET–PR(14)21

C. Giroud, S. Jachmich, P. Jacquet, A. Jarvinen, E. Lerche, F. Rimini, L. Aho-Mantila, N. Aiba, I. Balboa, P. Belo, C. Angioni, M. Beurskens, S. Brezinsek, F.J. Casson, I. Coffey, G. Cunningham, E. Delabie, S. Devaux, P. Drewelow, L. Frassinetti, A. Figueiredo, A. Huber, J. Hillesheim, L. Garzotti, M. Goniche, M. Groth, Hyun-Tae Kim, M. Leyland, P. Lomas, G. Maddison, S. Marsen, G. Matthews, A. Meigs, S. Menmuir, T. Puetterich, G. van Rooij, S. Saarelma, M. Stamp, H. Urano, A. Webster and JET EFDA contributors

Progress at JET in Integrating ITER-Relevant Core and Edge Plasmas within the Constraints of an ITER-Like Wall

Progress at JET in Integrating ITER-Relevant Core and Edge Plasmas within the Constraints of an ITER-Like Wall

C. Giroud[1], S. Jachmich[2], P. Jacquet[1], A. Jarvinen[3], E. Lerche[2], F. Rimini[1], L. Aho-Mantila[4], N. Aiba[5], I. Balboa[1], P. Belo[1], C. Angioni[6], M. Beurskens[1], S. Brezinsek[7], F.J. Casson[1], I. Coffey[8], G. Cunningham[1], E. Delabie[9], S. Devaux[1], P. Drewelow[10], L. Frassinetti[11], A. Figueiredo[12], A. Huber[7], J. Hillesheim[1], L. Garzotti[1], M. Goniche[13], M. Groth[3], Hyun-Tae Kim[1], M. Leyland[14], P. Lomas[1], G. Maddison[1], S. Marsen[10], G. Matthews[1], A. Meigs[1], S. Menmuir[11], T. Puetterich[6], G. van Rooij[9], S. Saarelma[1], M. Stamp[1], H. Urano[5], A. Webster[1] and JET EFDA contributors*

JET-EFDA, Culham Science Centre, OX14 3DB, Abingdon, UK

[1]*CCFE, Culham Science Centre, Abingdon, OX14 3DB, UK*
[2]*ERM-KMS, Brussels Belgium*
[3]*Aalto University, Association EURATOM-Tekes, Otakaari 4, 02150 Espoo, Finland*
[4]*VTT Technical Research Centre of Finland, FI-02044 VTT, Finland*
[5]*Japan Atomic Energy Agency, Naka Fusion Institute, Naka, Ibaraki 311-0193, Japan*
[6]*Max-Planck-Institut für Plasmaphysik, EURATOM Association, 85748 Garching, Germany*
[7]*EK-Plasmaphysik, Forschungszentrum Jülich, Association EURATOM-FZJ, Jülich, Germany*
[8]*Astrophysics Research Centre, Queen's University, Belfast, BT7 1NN, Northern Ireland, UK*
[9]*FOM-DIFFER, PO BOX 1207, 3430 BE Nieuwegein, The Netherlands*
[10]*Max-Planck-Institut für Plasmaphysik, Teilinsitut Greifswald, D-17491 Greifswald, Germany*
[11]*VR, Department of Physics, SCI, KTH, SE-10691 Stockholm, Sweden*
[12]*Instituto de Plasmas e Fusão Nuclear, Instituto Superior Técnico, Universidade de Lisboa, 1049-001 Lisboa, Portugal*
[13]*CEA, IRFM, F-13108 Saint-Paul-lez-Durance, France*
[14]*York Plasma Institute, Department of Physics, University of York, Heslington, York, YO10 5DD, UK*
** See annex of F. Romanelli et al, "Overview of JET Results", (24th IAEA Fusion Energy Conference, San Diego, USA (2012)).*

Preprint of Paper to be submitted for publication in Proceedings of the
41st EPS Conference on Plasma Physics, Berlin, Germany
23rd June 2014 – 23rd June 2014

ABSTRACT

This paper reports the progress made at JET-ILW on integrating the requirements of the reference ITER baseline scenario with normalised confinement factor of 1, at a normalised pressure of 1.8 together with partially detached divertor whilst maintaining these conditions over many energy confinement time. The 2.5MA high triangularity ELMy H-modes are studied with two different divertor configurations. The power load reduction with N seeding is reported. The relationship between an increase in energy confinement and pedestal pressure with triangularity is investigated. The operational space of both plasma configurations is studied together the ELM energy losses and stability of the pedestal of unseeded and seeded plasmas.

1. INTRODUCTION

ITER operation with high fusion gain ($Q_{DT} = 10$) is based on inductive 15MA plasmas in a type-I ELMy H-mode regime with a deuterium-tritium mixture. This ITER inductive scenario is based on a sufficiently normalised energy confinement ($H_{98(y,2)} \sim 1$) at a normalised pressure $\beta_N \sim 1.8$, high density compared to the Greenwald density limit n_{gw} ($n_{gw} = I_p/2\pi a^2$ with I_p the plasma current and the minor radius a; $f_{GW} = \langle n \rangle / n_{gw} \sim 0.85$) at high fuel purity ($Z_{eff} \sim 1.6$) [1]. The inductive scenario is based on integrating the above plasma performance for the confined plasma (core plasma) whilst keeping within divertor conditions compatible with the Plasma Facing Components (PFCs). ITER will have Beryllium (Be) PFCs at the main wall and tungsten (W) PFCs at the divertor for minimum impurity contamination of plasma together with minimum fuel retention. The challenge is in the integration of these plasma core requirements together with divertor conditions compatible with the PFCs, acceptable ELMS and to achieve stationary plasma for a duration of $t_{stat} \sim 400$s (i.e. 100 times the energy confinement time $\tau_E \sim 3.5$s [2]).

It is imperative to have edge conditions compatible with the Plasma Facing Components both in the inter-ELM phase and during ELMs. High divertor radiation from extrinsic impurity will be mandatory for compatibility of power load with the divertor targets in the inter-ELM phase. It is estimated that the inter-ELM peak power load at the divertor is 20 – 40MW.m^{-2} for attached conditions and needs to be reduced down to less than 10MW.m^{-2} for compatibility with the PFCs [3, 4]. Modelling indicates that to satisfy these demanding requirements regarding divertor power handling control, while providing appropriate He exhaust and maintaining an acceptably low core impurity concentration [5, 6], ITER has to operate with a partially detached divertor (only the region near the separatrix is detached – evidencing local pressure loss).Under these conditions 80% of the input power needs to be radiated. For the seed impurity, ITER plans to have the flexibility to use Ne, Ar and N_2 (or a mixture thereof) as seed gases. Chemically reactive species will be more of a safety challenge for the plant than a noble gas). In addition, The ELM energy will be restricted to be less than 0.7MJ, which corresponds roughly to $\Delta W_{elm}/W_{ped}$ below 1%, and will require active ELM control [7].

The pedestal is key to achieving the challenging integration of plasma core performances and divertor conditions compatible with the PFCs. The core plasma requirements necessitate a high

pedestal plasma density and temperature. Indeed, the energy confinement and fusion gain are strongly affected by the pedestal temperature due to profile stiffness. Also a high core plasma density is best achieved keeping the plasma density only moderately peaked with a high pedestal density to avoid MHD instabilities and impurity peaking. However, the pedestal temperature decreases with increasing pedestal density as the pedestal pressure is limited by ELMs to be a nearly constant value [1]. So for a value $H_{98(y,2)}$ of about 1 to be achieved at high density, improved pedestal pressure at high n_{ped}/n_{GW} is important. ITER inductive scenario is designed at high plasma triangularity $\delta \sim 0.4$. It relies on the improved pedestal stability of high triangularity plasma, for which the pedestal pressure is higher than in low δ discharges at a given pedestal density.

Achieving partially detached divertor conditions with extrinsic impurity whilst maintaining the requirement of $H_{98(y,2)} \sim 1$, $\beta_N \sim 1.8$ and high fuel purity is a challenge for the H-mode pedestal, in particular, due to the closeness of the operational point of the inductive scenario to the back-transition from H-mode to L-mode confinement. At present, the input power threshold for the inductive scenario is expected to be ~ 70MW and the power through the separatrix ~ 79MW [8]. It is expected that in ITER the reference inductive scenario operation will relatively close to the type-III operational boundary [10] as well as H to L threshold.

In this paper, we report progress made in integrating ITER-relevant core and edge plasmas within the constraints of an ITER-like wall at JET. The dynamic phase of the current ramp-up and ramp-down times and the requirements for active ELM control in impurity seeded plasmas will not be discussed in this paper. Also, in this paper the discussion is restricted to nitrogen (N) seeded plasmas. Nitrogen as an extrinsic radiator has a role to play in the development of radiative scenario in current devices for two important reasons: firstly, due to its lower ionisation energy it plays the role that neon will have under ITER divertor conditions where the pedestal will be hot ~ 3–4keV compared to ~ 1keV in JET, and secondly it isolates the effect that high divertor radiation power load reduction has on pedestal performance [11].

This paper is organized as follows: a description of the scenarios is given in section 2; the reduction of the power load to the divertor in section 3; the impact of the extrinsic radiation on energy confinement, pedestal pressure and dependence on plasma triangularity is discussed in section 4; the achievement of stationary plasma conditions is presented in section 5; section 6 will present the status of plasma integrated performance at JET and finally a conclusion will be given in section 7.

2. DESCRIPTION OF THE EXPERIMENTS

This paper concentrates on the baseline ELMy H-mode scenario at 2.5MA. The ITER baseline scenario [11] was selected as the reference scenario in JET on which to document the impact of a change of wall on plasma performance and on the power load to the divertor. This ELMy H-mode scenario in JET has a plasma field and current of 2.5MA/2.6–2.7T, $q95 \sim 3.5$, $P\text{in} \sim 16$MW, $\delta \sim 0.4$ (the average triangularity), $H_{98(y,2)} \sim 1.0$. The divertor geometry of the chosen configuration has

the inner strike on the vertical divertor target and the outer strike on the horizontal divertor target as shown in Fig 1a. In this paper, these plasmas will be referred as JET-C high-δ HT plasmas, i.e high-δ horizontal target divertor plasmas. Deuterium and nitrogen were injected at the divertor target respectively from the high-field side (HFS) divertor target and from the low field side into the common-flux region, as discussed in more details in ref [12]. In JET-ILW, similar discharges were repeated at 2.5MA/2.65T, $\delta \sim 0.37$, Pin ~ 15–17MW, with a similar divertor geometry as shown in Fig 1a. These plasmas will be referred to in this paper as JET-ILW high-δ HT plasmas. The JET-C and JET-ILW high-δ HT plasmas correspond to the best set of ELMy H-mode discharges that document the change of wall in terms of pedestal characteristics and power load for a range of pedestal densities.

In addition, a low triangularity plasma was developed for JET-ILW, here referred to as low-δ HT plasmas, with similar divertor geometry as the high-δ HT as seen in Fig 1b and a similar plasma volume, see Table 1. Also in order to investigate the impact of the divertor geometry, low and high-δ plasmas with both inner and outer strike on the vertical targets have been developed, referred to respectively as low-δ and high-δ VT plasmas , see Figs 1c and 1d. The positions of deuterium and nitrogen injection were unchanged with respect to JET-C high-δ HT plasmas. The divertor configuration of VT plasmas is more closed to neutrals than that for the HT plasma and more similar to the ITER divertor . More information can be found in Table 1 and in Refs [12, 13].

In most tokamak devices with carbon- fibre composite (CFC) as plasma facing materials, it was observed that in high triangularity δ plasmas, it was possible to maintain a higher edge pedestal pressure with fuelling at high $<n_e>/n_{GW}$ than in low δ discharges [14, 15, 16], due to the improved MHD stability of the pedestal. In JET it was even observed that for the selected reference scenario (JET-C high-δ HT) at high triangularity, a high energy confinement $H_{98(y,2)} \sim 0.9–1$ at $<n_e>/n_{GW}$ could be achieved with fuelling and is linked to the mixed type-I/II ELMy regime characterized by higher pedestal pressure than pure type-I ELMs [11]. Other devices did see an improvement of pedestal pressure with triangularity at a given $<n_e>/n_{GW}$ but in all cases the global energy confinement drops as the edge density is increased with fuelling, unlike the ITER baseline scenario case at JET [11].

3. ACHIEVEMENT OF PARTIAL AND FULL DETACHMENT IN JET-C AND JET-ILW

Divertor detachment can lead to a significant reduction of the power arriving at the outer divertor target (OT) can be achieved with respect to the power flowing through the separatrix (P_{sep}). These conditions are obtained by lowering the plasma temperature at the OT either by decreasing the separatrix temperature or by radiation from seed impurities in the scrape-off-layer (SOL) and divertor. Below the power load at the outer strike are discussed only as the inner strike point is fully detached.

In JET-C, it was possible in the high-δ HT plasmas (introduced in section 2) to reach partial detachment with fuelling alone [12, 19] at fuelling rate of 2.8×10^{22}el/s (Pulse Number: 76678).

Although modelling with the EDGE2D-Eirene code of these JET-C discharges established that it was through an increased C (carbon) divertor radiation [17] induced by increased D sputtering and not D radiation alone. The radiative fraction f_{rad} (P_{rad}/P_{in} with P_{rad} the total radiated power and P_{in} the input power) only modestly increased from 0.44 (Pulse Number: 76666) for the reference low fuelled discharge (with attached divertor conditions) to 0.55 (Pulse Number: 76678) for partially or even detached divertor conditions, with a ratio $P_{rad,div}/P_{rad,main} \sim 0.7$ (with $P_{rad,div}$ and $P_{rad,main}$ being the radiated power in the divertor and in the main plasma, respectively). A higher radiative fraction was therefore not necessary to achieve the required divertor conditions. Both in attached and partially detached divertor conditions, the divertor radiation was located at the X-point as shown in Ref [12].

In JET-ILW, the strong reduction of the C concentration by a factor of 10 [18] led to reduced divertor radiation and subsequent higher divertor power load. In JET-ILW, the high-δ HT plasma with a fuelling rate of 2.8×10^{22}el/s and input power similar to the JET-C reference pulse (Pulse Number: 76678) is repeated. Whereas the divertor conditions were partially detached in JET-C [12], the divertor remained in attached conditions in JET-ILW (Pulse Number: 82806) as shown for the unseeded case in Fig 2a. The power load increased from JET-C to JET-ILW from 0.22 to $0.3 \times$ Psep and the plasma temperature at the divertor target increased from ~ 5eV to 26eV [13], due to the absence of C as intrinsic radiator. The radiative fraction decreased from $f_{rad} \sim 0.55$ and $P_{rad,div}/P_{rad,main} \sim 0.7$ in JET-C (Pulse Number: 76678), down to ~ 0.3 with $P_{rad,div}/P_{rad,main} \sim 0.3$ [13] in JET-ILW (Pulse Number: 82806).

It was shown for JET-ILW in [13] that, independently of the fuelling rate, and with a high enough N-seeding rate, similar conditions of $f_{rad} \sim 0.55$ and value of the ratio $P_{rad,div}/P_{rad,main} \sim 0.7$ can be obtained resulting in very similar reduction in the power load at the OT target compared to the JET-C reference pulse (Pulse Number: 76678) and with the radiation again located at the X-point. Figures 2a) and b) show that in high-δ HT plasmas at increasing N-seeding levels , the ion current decreases and temperature drop at the strike point divertor, both signs of partially detached divertor conditions. In high-δ VT plasmas, divertor conditions of partial detachment were also reached as shown in Figs 2c and 2d. In fact, it was shown for both divertor configurations that if the radiative power in the divertor was about 40% of P_{sep} in high-δ HT plasmas, the power reaching the OT will be substantially reduced and the divertor conditions will be partially detached, see figure 3. It was found that this figure of merit ($P_{rad,div} \sim 40\%$ of P_{sep}) is also a sufficient condition for achieving these conditions in the JET-C high-δ HT plasmas (not shown here) as well as for the JET-ILW high-δ VT plasmas, see Fig 3.

EDGE2D-EIRENE modelling of high-δ HT plasmas in JET-ILW has been carried out. Reference [20] demonstrates that EDGE2D-EIRENE was able to capture the detachment processes induced by N as measured in experiment for both power and ion current at the outer target. Similar to the experimental observations, in the simulations a factor 10 reduction in divertor power load was obtained when the divertor radiation is about 50% of P_{sep}. Finally, the peak outer divertor power and particle

flux reduction in the nitrogen induced detached conditions is obtained almost solely via nitrogen radiation, and associated reduction in the power flow to the deuterium ionization and recycling front. As a result, the divertor particle fluxes in detachment are reduced without the need for strong recombination sink for particles in front of the targets, highlighting that the processes in impurity injection induced detachment can be different than in deuterium fuelling induced detachment.
Moreover, it is compulsory in ITER scenarios to have edge conditions compatible with the PFCs not only during the inter-ELM period but also during the ELMs. With N injected for inter-ELM power-load reduction, the ELM energy losses and frequency can have a complex behaviour as a result. It is important to stress that no difference for the energy deposition fluency ε_{ELM} during an ELM ($kJ.m^{-2}$) was observed between JET-C and JET-ILW and the peak deposited energy fluency remains dependent on the pedestal pressure [22]. The ELM energy losses will be discussed in section 4c as part of the description of the operational space of seeded high-δ HT and VT plasmas.

4. CONFINEMENT DEPENDENCE OF HIGH-δ PLASMA ON IMPURITY

From the previous section it might be inferred that the change of wall material had not particularly impacted the energy confinement of high-δ HT plasmas. This is far from being the case. In this section, the global confinement and pedestal pressure of high triangularity plasmas is discussed, and a comparison with low triangularity plasmas is given.

4A. ENERGY CONFINEMENT AND PEDESTAL IN FUELLED AND SEEDED HIGH-δ HT PLASMAS IN JET-ILW

Similar discharges were repeated in JET-ILW to those reference high-δ HT plasmas in JET-C presented in section 2. It was expected that tungsten (W) contamination in the main plasma would limit operation at low density due to both high W source resulting in excessive main plasma radiation, and to excessive divertor power load due to the lack of C as an intrinsic radiator.

It came as a surprise however that at higher pedestal density the same performance of $H_{98(y,2)} \sim 0.95$, $\beta_N \sim 1.9$ (as for Pulse Number: 76678) could not be achieved when the scenario was repeated in JET- ILW, [13, 23]. In Figure 4 with the same net power of $P_{net} \sim 10MW$ ($P_{net} = P_{in} - P_{rad,main}$), a reduction in stored energy was observed of up to 40% and $H_{98(y,2)} \sim 0.7$, $\beta_N \sim 1.1$ (Pulse Number: 82806) [13] while still featuring type-I like ELMs with large ELM-energy losses, see section 4f. The reduction in stored energy stems from a reduction in the pedestal pressure and mostly the pedestal temperature as shown in Fig 5 [13].

Numerous ideas were raised on the possible reason for this reduction in stored energy: increased core radiation due to W leading to a decreased power flowing through the separatrix (P_{sep}), ion dilution effect [24], a change in core transport where the lack of impurities could affect the core gradients [25], or an additional energy loss channel in ILW than in JET-C via neutrals [26]. None of these mechanisms proved to fully describe the observed changes in confinement. Specifically in

this scenario at $n_{e,ped}/n_{gw}$ being an almost exact repeat of a JET-C scenario it is possible to answer the following. The drop in confinement in the JET-ILW plasma compared with that of the JET-C cannot be attributed to an increased main plasma radiation due to W, see figure 2 in reference [13]. Modelling has been carried in EDGE2D-EIRENE and show that in fact the D_0 flux across the separatrix increases with increasing divertor radiation for the high-δ HT configuration. As a result, in the unseeded JET plasmas, the neutral fuelling through the separatrix in JET-C is predicted to be 20% higher than in the JET-ILW plasmas. The details of this work will be reported in [27].

The absence of C seems to have substantially affected the pedestal. An additional unexpected observation is the fact that the JET-ILW plasmas with type-I like ELMs, such as Pulse Number: 82806, exists below the critical electron pedestal temperature for type-III ELMs in JET with a carbon wall at high densities as shown in Figure 5. In order to identify the position of the back-transition from type-I to type-III ELM regime for the 2.5MA plasma in JET-ILW, power ramp-down scans were performed in JET-ILW, see Figure 6. The transitions appears at reduced pedestal temperature at a $T_{e,ped} \sim 0.35$keV for $n_{e,ped}/n_{gw} \sim 0.85$ (Pulse Numbers: 82283, 82290). The boundary between type-I and type-III ELM regimes, which was such a key player in both ELM dynamics and drop in confinement in JET-C discharges as a result of seeding [12], seems to lie far below its previous position at $T_{e,ped} \sim 0.7$keV, shown in Figure 5. In addition the triangularity seems to have no beneficial effect on the pedestal pressure as discharges with a similar pedestal density and different triangularity have a similar pedestal pressure as shown in reference [28] and illustrated in fig 5 with unseeded high and low-δ HT plasmas. Major changes seem to have taken place in the behaviour of the high-δ plasma pedestal with a change of the plasma facing materials.

Although nitrogen was first injected to increase divertor radiation and reduce power loads, nitrogen seeding has been found to improve plasma energy confinement in the high-δ HT plasma [13]. When nitrogen is injected into deuterium-fuelled high-δ HT plasmas in JET-ILW, it raises the pedestal density and temperature leading to an increase in stored energy to 5.5MJ close to the JET-C fuelled counterpart [13], which had a stored energy of 6MJ. It was unexpected that N-seeding lead to an increase of the H-mode pedestal pressure, mainly temperature, partially recovering the pedestal pressure of unseeded JET-C high-δ HT plasmas as shown in Fig 4. N_2 was also seeded in the low-δ HT plasma but the improvement in pedestal pressure was not as prominent as shown in Figure 5. The improvement of confinement at high-δ HT with respect to low-δ HT plasmas at a given pedestal density seems to have been re-established with nitrogen seeding [28].

4B. EFFECT OF N-SEEDING AND PLASMA TRIANGULARITY ON ENERGY CONFINEMENT IN PLASMA WITH VERTICAL DIVERTOR TARGETS

As mentioned in section 2, the high-δ HT plasma configuration in JET-C had the peculiar behaviour to keep at high $\langle n_e \rangle/n_{GW}$ a similar confinement ($H_{98(y,2)} \sim 1$) than at low $\langle n_e \rangle/n_{GW}$, unlike observations make on other devices [11]. Therefore, we want to verify that the increase in pedestal pressure with N is linked to the high triangularity and not specific to the high-δ HT configuration. In this

section, we compare the confinement response to seeding in VT plasmas with both low and high triangularity plasma shaping.

An experiment was conducted in VT plasmas where the plasma triangularity was changed from high $\delta \sim 0.22$ to low $\delta \sim 0.36$ whilst keeping the vertical target divertor configuration unchanged as well as using the same heating, fuelling and seeding waveforms. Figure 6 illustrates that without N seeding an increase of the plasma triangularity raises the density, but does not improve the stored energy in VT plasmas, illustrating a similar result to the one observed in HT plasmas [28]. However, N seeding In low-δ VT plasma increases the stored energy by 15% whereas in high-δ VT plasma, N seeding increases the stored energy by 40%, see Fig 7. No reference exists for this configuration in JET-C. These results clearly established that in JET-ILW, the increase in confinement with N-seeding is dependent on the plasma triangularity and not plasma configuration.

4C. OPERATIONAL SPACE OF HIGH-Δ DISCHARGES WITH N SEEDING IN JET-C AND JET-ILW

Before investigating the change in pedestal characteristics in high-δ HT and VT plasmas with nitrogen seeding, the operational space of the high-δ HT and VT plasmas are compared and put in context with the their JET-C counterparts.

The operational space of fuelled JET-C high-δ HT plasmas was already reported in previous papers [29, 30, 12, 19]. The operational diagram of H_{98} versus $n_{e,ped}/n_{GW}$ for the JET-C high-δ HT plasmas is shown in Figure 9 for a scan in fuelling from 0 to 6×10^{22} el/s rate at constant input power (Pin ~ 16MW) operating at $P_{sep}/P_{LH,ITER} \sim 1.2$. At low fuelling ($\Gamma_D \sim 0.4 \times 10^{22}$el/s), $H_{98(y,2)} > 1$ (Pulse Number: 76666) can be achieved. When the fuelling is increased to $\sim 3 \times 10^{22}$el/s, the pedestal density increases to the Greenwald density limit, and a good normalised confinement $H_{98(y,2)} \sim 0.95$ can still be achieved. At this high density the plasma has made a transition from pure Type I to mixed Type I/II ELMs [11] (Pulse Number: 76678 in Fig 7).

Details of the plasma performance, ELM energy losses and frequency are shown in Table 2. As the fuelling is further increased towards 6×10^{22}el/s, the density decreases and the plasma will eventually make a transition to the type-III ELM regime [9] with $H_{98(y,2)} \sim 0.8$, as shown in Figure 9. As discussed in [12, 30] and [19], in JET-C seeding nitrogen does not have a beneficial effect on the confinement and leads to a reduction of the pedestal density and normalized confinement as shown in Fig 9. Starting from the unseeded discharges Pulse Number: 76678, the ELM frequency increases as the N-seeding rate is increased from $0–1.5 \times 10^{22}$el/s (Pulse Number: 76680) in successive discharges. Finally at the highest N-seeding rate of 3×10^{22}el/s, the pedestal temperature $T_{e,ped}$ is reduced and the plasmas make a transition to the Type III ELM regime with a reduced pressure gradient and a degradation of the confinement with $H_{98(y,2)} \sim 0.78$, $n_{e,ped}/n_{GW} \sim 0.7$ (Pulse Number: 76681). For lower fuelling rate, the same picture applies at nitrogen seeding rate is increased as shown in Fig 9. In JET-C, the transition from type-I to type-III ELM regime turned out to be the limitation in achieving high divertor radiated power and H- factor close to 1 [12].

The high-δ HT plasmas have a reduced energy confinement in comparison to JET-C. As nitrogen is injected with a constant fuelling rate of ~ 2.8×10^{22}el/s, the energy confinement is partially recovered and the ELM energy losses are increased and ELM frequency decreased (Pulse Number: 82810, see Table 2). If the nitrogen seeding is further increased, a similar trajectory in $n_{e,ped}/n_{GW}$ versus $H_{98(y,2)}$ diagram to the one observed in N seeded JET-C plasmas is obtained (as shown in Fig 9 and also in ref [13]) and the pedestal density decreases, the ELM energy losses decreases, the ELM frequency increases and the energy confinement is reduced (e.g. Pulse Number: 82811, see Table 2). The high-δ VT plasmas have been added to the operational diagram in Fig 9. The target D-fueling level for the high-δ VT plasmas (Pulse Numbers: 85263, 85262) has been selected to obtain the same ELM averaged pedestal density (~ $7 \times 10^{19}m^{-3}$) as the high-δ HT plasma reference Pulse Number: 82806. Similar ELM energy losses and frequency are obtained with a similarly low normalized confinement, see Table 2. The energy confinement in this configuration is also improved with N-seeding. Fig 9 shows that as the N-seeding rate is increased the normalized confinement is increased. However, the ELMs size reduced in size and become more frequent (Pulse Numbers: 85266, 85270); see Pulse Numbers: 85262 and 85263 in Table 2. Opposite trends are observed for the pedestal density, which increases for high-δ HT plasmas whereas it decreases for the high-δ VT plasmas. In fact, plamas with vertical target divertor geometry provide better control of the pedestal density than with a horizontal target configuration whilst maintaining the core plasma performance of high-δ N-seeded plasmas. It is likely that the difference in behavior in electron pedestal density is linked to the difference in divertor geometry and its effect on neutral recycling.

It is now possible to identify from this operational domain with the information obtained on power load in section 3, the best candidates for an integrated plasma performance scenario, i.e. as high as possible normalized confinement, high density $f_{GW} \sim 0.85$, a partially detached divertor and tolerable ELM energy losses (as a criteria $\Delta W_{helm}/W_{iped} < 5\%$ is chosen in this paper, as this is the detection limit of the stored energy measurements). The best candidates from the high-δ HT plasmas are Pulse Number: 76687 in JET-C, Pulse Number: 85412 in high-δ HT and in Pulse Number: 85419 in high-δ VT plasmas in JET- ILW. It can be seen from Table 2, that these plasma performance are in fact fairly similar with $H_{98(y,2)} \sim 0.86$, $n_{e,ped}/n_{GW} \sim 0.6$-$0.76$, $\beta_N \sim 1.5$–1.6 for these plasmas. Future experiments will have to address whether at higher input power the normalised confinement and pressure could be raised whilst maintain small ELMs and partially detached divertor conditions.

4D. PEDESTAL STRUCTURE AND STABILITY OF N-SEEDED DISCHARGES

Nitrogen seeding increases the energy confinement in both high-δ HT and VT plasmas. In both cases the increase is due to an increase in pedestal pressure as shown in Figure 5 [13]. More information can be obtained with the identification of common features between the two configurations. For both high-δ HT and VT configurations the ELM-averaged pedestal pressure and temperature increase as a result of the seeding, as shown in Figure 10. However, opposite trends are observed for the

average pedestal density, which increases in the high-δ HT plasmas whereas it decreases in the VT plasmas. At the seeding rate of $\Gamma_N \sim 2.5–3 \times 10^{22}$el/s, the relative increase in pedestal pressure is a factor ~ 1.6 in both configurations from their respective unseeded references. For the high-δ HT plasmas, the increase in pressure is due to a similar increase in density and temperature, i.e a factor 1.2 versus a factor 1.35 respectively. Whereas for the high-δ VT plasmas, the net increased pressure is due to an increased temperature (factor 1.9) as the density decreases (by a factor 0.85). The pre-ELM pedestal electron pressure, temperature and density are shown in Figure 11. For the high-δ VT plasmas, the pedestal pressure still show a small increase with N injection but not as large an increase as seen from the ELM-averaged pedestal values, and not enough to explain the increase in global confinement. This difference is due to a reduction of the ELM energy losses with N seeding for high-δ VT plasmas, presented in section 4c. Nevertheless, the common feature between the seeded high-δ HT and VT is the increase in pedestal pressure due to an increase in pedestal temperature with respect to the unseeded reference discharges. This trend is most clear in the pre-ELM averaged pedestal data. Any future mechanism proposed for the increase in pedestal pressure with N injection will have to reproduce the trend in Figs 10 and 11.

4E. PEELING-BALLOONING STABILITY OF HIGH-δ PLASMAS, ELMS SIZE AND ELM IDENTIFICATION

The unexpected decrease in pedestal pressure for unseeded high triangularity plasmas has challenged our understanding of the pedestal stability for high triangularity plasmas. It is still not know what mechanisms lead to low pedestal pressure in unseeded high-δ plasmas in JET-ILW with respect to JET-C, and what mechanisms lead with N to an increase pedestal pressure in high-δ plasmas in JET-ILW. The current idea being investigated for high-δ plasmas is that the pedestal structure and stability are affected by a change in fuel recycling and decrease in C content.

In this section, we would like to verify whether the pedestal pressure of high-δ plasmas in JET-ILW is indeed limited by the Peeling-Ballooning (PB) instabilities. A concise summary on how the PB stability is calculated is first given, more details can be found in [34, Leyland 2013] and references therein.

In the PB model the pedestal MHD stability is limited by current driven low n-number (n = 1–5) peeling modes and pressure gradient limited high n-number (n > 20) ballooning modes. The intermediate n-numbers (n = 5–20) are limited by combined peeling-ballooning modes. The PB model has been successfully tested in many tokamaks where high spatial resolution profiles are available of the pedestal electron and ion temperature, density and the impurity content [DIII-D, JET, AUG, JT- 60U]. The determination of the PB stability analysis requires an ideal MHD eigenvalue solver such as MISHKA-I [31] and ELITE [32, 33]. The input data for this analysis is the total pressure profile P and edge bootstrap current profiles (J_{ped}) (within plasma region $0.85 \geq \psi_n \geq 1.1$) and plasma equilibrium. The total pressure profile is determined from the experimentally measured ion and electron temperature and density with $P = n_e T_e + n_i(n_e, z_{eff})$. The edge current profile, not

routinely measured in most tokamaks, is derived from the kinetic profiles using the Sauter formulae [35]. In this paper, and common for PB analysis at JET, the plasma equilibrium is self-consistently calculated with the HELENA equilibrium solver.

The PB stability is affected both by global pressure and plasma shaping. Increased global pressure renders the ballooning modes stable at higher pressure gradients. Increased plasma triangularity is expected to increase pressure gradients at high edge currents. At increased triangularity the PB stability can be extended to higher pedestal pressure only if sufficient edge current (J_{ped}) can be sustained. At low edge current this benefical effect of plasma triangularity is reduced. For convenience, the region of enhanced pedestal pressure gradient for increased edge current in the PB diagram will be colloquially referred to as the 'corner' in the PB diagram in the further discussion. This is the region that we want to access to achieve high pedestal pressure at high value of $n_{e,ped}/n_{GW}$. Due to the coupling of edge current and pedestal pressure gradient through the bootstrap current [35], access to the corner of the PB diagram depends on plasma collisionality. Unlike for type-I ELMy H-mode plasma, the pedestal of type-III ELMy H-mode is found not to be limited by PB stability.

A first attempt to verify if the pedestal pressure of high-δ plasmas in JET-ILW fuelled or seeded are indeed limited by the PB instabilities was reported in [28], SaarelmaHMWS2013]. Across a fuelling scan the pedestal moved from ballooning unstable to being fully stable with respect to PB modes, whereas the pedestal top pressure remained unchanged. All these plasmas featured type-I like ELM behaviour with large ELM energy losses, as is shown in Fig 12 and in Table 2 . Figure 12 shows the time traces of the stored energy for a few examples indicating that experimentally these plasmas appear in type-I like ELMy H-mode with large ELM energy losses across the fuelling scan. In [28, SaarelmaHMWS2013] this observation questioned the validity of the Peeling Ballooning model in its description of type-I ELMy H-mode pedestal stability.

Here we report on improved analysis of the PB stability of these plasmas. In previous studies of the pedestal stability it was found to be sufficient to analyse only up to n = 30 in the ELITE MHD stability code. However, the unseeded high-δ HT plasmas presented here feature cold pedestals with high collisionality, and therefore low edge current. It was found necessary to go up to higher n-number in the PB analysis. Figure 13 shows the PB analysis with $n \leq 50$ and even one example with $n \leq 70$ using otherwise the same input parameters and kinetic profiles as in Figure 13 of [28], which only went up to n = 30. It is clear from the comparison of the two figures that in the new analysis the slope of the ballooning boundary steepens and that the boundary moves towards the experimental data. There is still a degree of uncertainty in this analysis, as the ballooning stability at high collisionality may require PB stability calculations to even higher n-numbers. Nevertheless, this analysis makes it plausible that the JET-ILW unseeded high-δ HT plasmas are indeed PB limited. Figure 13 also shows why triangularity seems to have no beneficial effect on the pedestal pressure of unseeded discharges, see Figures 5 and 7. Due to the high collisionality of these plasmas, the pedestal has a lower J_{ped}–α_{max} trajectory (j_{ped} being the edge current and α_{max} the dimensionless

normalized pressure gradient) which meets the ballooning boundary at reduced pressure gradient α_{max}. Similarly to the high-δ HT plasmas, the unseeded high-δ VT plasmas also feature large type-I like ELMs as shown in Figure 14. The operational points of these high-δ VT pedestals in the j_{ped}–α diagram show that their pedestal are marginally stable with respect to the ballooning boundary, see Figure 15. In both configurations, the unseeded plasma is PB limited and in type-I ELM but the total stored energy is low.

The same PB stability analysis was carried out for the seeded high-δ HT plasma. Figure 16 shows the stored energy of such plasmas, all at higher stored energy than the unseeded cases. The plasma with the highest stored energy (Pulse Number: 82817) has considerable ELM energy losses (150kJ) at low ELM frequency (20Hz), a signature of the type-I ELM. The pedestal of the Pulse Number: 82817 plasma is PB limited. The operational point approaches the corner of the PB diagram, for the plasma to fully benefit from plasma shaping with high triangularity, possibly due to the increased temperature pedestal height.

An additional interesting comparison is given by the Pulse Numbers: 85412 and 85413. The Pulse Number: 85412 has a slightly lower pedestal pressure and lower total stored energy at the same seeding and fuelling level but different input power. The time traces in Figure 16 reveal that this pulse also has a very different ELM behaviour with a much higher ELM frequency (48Hz) and very small ELM energy losses (65kJ), reaching the W_{MHD} detection limit. Nevertheless, its total stored energy is significantly higher than the unseeded pulses in Figure 12. The picture emerges that this pulse could no longer be in the type-I ELM regime but features type-III ELMs. The dependence of ELM frequency with input power, in Fig 18, exhibit a bifurcation characteristic of a transition to type-III ELM regime [9]. This observation is further strengthened by Pulse Number: 82819 that lies between the two pulses in terms of stored energy. It also features a mixed ELM regime that resemble the mixed type I-III ELM characteristics that occurred in JET-C at the transition from pure type-I to pure type III ELMs, see Figure 18 [9, 12]. At the level of accuracy, available from the JET measurements, the PB stability diagram can only qualitatively contribute to the identification of ELMs in Pulse Number: 85412 as type-III ELMs; Figure 17 shows that Pulse Number: 85412 lays removed from the stability boundary, be it that it is in an area where high n-numbers are required (here $n < 50$ is used). Type-III ELMs are usually found not to be limited by the PB stability.

The comparison of unseeded and seeded plasmas in the high-δ VT plasmas is even starker; For the seeded plasmas the stored energy is increased in relation to the unseeded reference discharges, as illustrated by the stored energy in the time traces in Figs 14 and 20. Nevertheless, the ELM characteristic resembles that of Type III ELMs in the W_{MHD} time traces (apart from Pulse Number: 85266, which resembles a more compound Type I/III ELM behaviour). A rather sharp decline in ELM frequency with input power, Figure 19, also indicates the signature of Type III ELMs. This is confirmed by the PB stability analysis as seen in Figure 21, as the experimental points in the stability diagram are far removed from the ballooning boundary; another indication that these plasmas are in type-III ELMy H-mode.

4F. DISCUSSION

In JET-ILW, it was shown that in unseeded high-δ ELMy H-mode plasmas in two divertor configuration with horizontal (HT) and vertical divertor targets (VT) at 2.5MA , the plasma triangularity has no beneficial effect on the pedestal pressure. Nevertheless for both high-δ configurations, the unseeded plasmas have pedestal pressure gradient limited by Peeling Ballooning (PB) stability and are in type-I ELM regime. The stored energy remains low with respect to the type-I ELMy H-mode plasma in JET-C. The low pedestal pressure in the highly fuelled HT and VT plasmas is understood by their location in the PB diagram. As the collisionality of these plasmas is high, only a low bootstrap current can be maintained and the stability boundary is met at reduced pressure gradient α_{max}. At such low edge current, the improved pedestal stability at high triangularity, in the corner of the PB diagram, is not accessible in high fuelled JET-ILW plasmas and the benefit of high triangularity at high $n_{e,ped}/n_{gw}$ on the pedestal stability is lost. Low-δ and high-δ plasmas have the same pedestal pressure. However for unseeded high-δ HT plasmas the pedestal confinement is low across a wide fuelling range, whereas the low fuelling plasmas are close to the corner of the stability diagram, see Figure 13 (there is no low fuelled high-δ VT plasmas at present). This was already explained in [Leyland2014, [28] (and not readdressed here as a result) and is due to a complex change in pedestal structure; the low fuelling plasmas feature a narrow pedestal and steep pressure gradients, whereas the high fuelling plasmas feature a wide pressure pedestal and shallow gradient. As a result the high-δ HT plasmas feature the same low pedestal pressure across the fuelling scan. The improved pedestal pressure of high triangularity plasmas in JET-C is thought to be linked to the presence of C – an effect that could not have been studied due to the inherent presence of carbon. The mechanism that leads to low pedestal pressure for unseeded high-δ plasmas in JET-ILW has not been yet identified, but has to be linked to a change of recycling and lack of impurity that affects the pedestal structure and stability.

Seeding nitrogen in JET-ILW plasmas (at 2.5MA) increases the energy confinement and pedestal pressure in both high-δ HT and VT plasmas. It was shown that N seeding re-establishes the dependence of energy confinement with triangularity for both configurations. Here again, the mechanisms for N seeding to increase pedestal pressure is not known, but it has to be linked to an increase in pedestal temperature – a common feature of the increase in pedestal pressure in high-δ HT and VT plasmas with N seeding. For one of the configuration, the reduction of the ELM energy losses plays an important role in the increase of pedestal pressure with N seeding.

The dependence of ELM energy losses with N seeding can be complex depending on the nitrogen seeding rate and divertor configuration. In the high-δ HT plasmas at 2.5MA, for a given fuelling rate, the ELM energy losses will first increase as N seeding is raised, with a pedestal that is PB limited and large type-I ELMs at low frequency. At high N seeding rate, the ELM energy losses will decreases down to ~ 80kJ and the pedestal become stable with respect to PB instabilities. For the high-δ VT plasmas, as N seeding is increased, the ELM energy losses decrease down to ~ 50kJ. The pedestal pressure is not limited by PB instabilities. Key to this difference in ELM energy losses with

N seeding is the pedestal density. As nitrogen is seeded, the pedestal density increases in high-δ VT plasmas whereas it decreases in high-δ VT plasmas, most likely linked to the difference in divertor geometry and its effect on neutral recycling. This means that the high-δ HT plasmas are at $n_{e,ped}/n_{GW}$ greater than 0.75 whereas the high-δ VT are at $n_{e,ped}/n_{GW}$ less than 0.6. If the same boundary as in JET-C applied in JET-ILW between type-I and type-III ELM regime in the $T_{e,ped}$–$n_{e,ped}$ diagram, the high-δ VT plasmas would be in type-III ELM regime and the high-δ HT plasmas in type-I at medium seeding rate and close to type-III ELM regime at high seeding rate, see Fig 5.

In section 4a, it was shown that in unseeded JET-ILW the type-I to type-III transition occurs at much lower pedestal pressure compared to JET-C plasmas. The transitions appears at reduced pedestal temperature at a $T_{e,ped} \sim 0.35$keV for $n_{e,ped}/n_{gw} \sim 0.85$ instead of $T_{e,ped} \sim 0.7$keV at same or $n_{e,ped}/n_{gw}$ for JET-C for a similar value of $n_{e,ped}/n_{gw}$. This transition is lifted back to increased pedestal pressure when N is seeded. This means that N-seeding increases the critical pedestal temperature for transition from type I to type-III ELM regime from ~ 350eV to above ~ 700eV and back to the boundary found in JET-C [12], see Fig 5. This new observation is important to understand the confinement of seeded discharges in JET-ILW.

Seeding nitrogen in the high-δ HT plasmas at 2.5MA in JET-ILW re-establishes the improved pedestal stability at high triangularity plasmas and the corner of the PB stability is once again accessible. For the HT configuration a decrease in collisionality by an increase in pedestal temperature has given renewed access to the corner of the PB diagram at high normalised pressure gradient α_{max}, as is seen in Figure 17. The increase in pressure gradient has allowed access to increased pedestal pressure and better confinement ($W_{MHD} \sim 6$MJ, e.g. Pulse Number: 82817). This is possible because the N-seeded plasmas at relatively high fuelling and seeding level combine a high pressure gradient with a wide pedestal and thus leading to an improved pedestal pressure [Leyland2014, [28]. These plasmas feature relatively large type I ELMs (~ 150kJ/ELM) for a given fuelling and seeding rate. When N seeding is further raised, the ELM energy losses decrease and a likely transition occurs from Type I to type III ELMs with small ELM energy losses; the pedestal then becomes stable with respect to PB instabilities. Nevethess these plasmas still feature an improved pedestal pressure with respect to the unseeded plasmas; e.g. compare Pulse Number: 85412 with $W_{MHD} = 5.1$MJ in Fig 16 with the pulses in Figure 12 with $W_{MHD} = 3.5$–4MJ. An improved pedestal pressure at high $n_{e,ped}/n_{GW}$ is once again possible.

The seeded high-δ VT plasmas have an improved confinement compared to the unseeded pulses. Unlike the high-δ HT plasmas, this improvement is not due to improved pedestal stability. The pedestal of seeded high-δ VT plasmas has been found to be stable with respect to the PB instabilities. The increase in average pedestal pressure is mostly due to the ELM energy losses with nitrogen seeding as is seen Figs 10 and 11. These seeded plasmas feature small ELMs (down to ~ 50kJ/ELM) and are in type-III ELM regime. Further work will be needed to understand why the dependence on triangularity of confinement is then maintained.

These results leads to the paradoxical situation that in the metallic JET-ILW, N-seeded plasma

with type-III ELMs have a better confinement and increased pedestal pressure than unseeded JET-ILW plasma in type-I ELM regime at 2.5MA/2.7T for high-δ VT and HT plasmas, not unlike results reported in [36]. However, it remains that with N seeding, the pedestal pressure obtained is not recovered for the same input power at same or $n_{e,ped}/n_{gw.}$

Future experiments will need to confirm that a raised power or increased pedestal pressure, the confinement can be raised and high-δ VT seeded plasma in type-I ELM can be obtained in JET-ILW. The high-δ VT plasma do however already offer even with their current global confinement an attractive integrated plasma performance as will be shown in section 6.

ITER inductive scenario is designed at a triangularity $\delta \sim 0.4$ to benefit from the improved pedestal stability of high triangularity plasma. It is still under debate if the ITER pedestal will be unstable with respect to the peeling instabilities or the ballooning instabilities [37, 38] and therefore if the ITER pedestal will be in a similar region of the PB diagram as JET is. Our understanding of high triangularity plasmas has been challenged by the unexpected decrease in pedestal pressure. The pedestal stability of high-δ plasmas has been affected by a change in fuel recycling and decrease in C content. In JET-C, the intrinsic seeding of C was playing a role in the improved stability of high triangularity plasmas via a mechanism that has not yet been identified, but is set by a combination of obtainable pedestal width and location in the PB diagram that allows high pressure gradients.

5. ACHIEVEMENT OF STATIONARY PLASMA CONDITIONS

In this section, we discuss the main difficulty we encountered to maintain stationary plasma conditions in the N-seeded high-δ ELMy H-modes and how we succeeded in solving it with application of core deposition of radio- frequency heating.

At the end of the first ILW campaign, it was reported that the N-seeded high-δ HT plasmas had good plasma performance, close the ITER requirements, but plasma conditions were not stationary ($t_{stat}/\tau_E \sim 6$) as is illustrated in Figure 22 for Pulse Number: 85413. The electron temperature in the plasma centre ($r/a < 0.3$) decreases and the sawtooth (ST) eventually disappear. Once the ST have disappeared, the plasmas will disrupt either during the main heating phase or during the plasma termination as is the case for Pulse Number: 85413 [40]. The same difficulty is observed in maintaining stationary conditions for high-δ VT plasmas as illustrated in Fig 26. It is important to note that both the high-δ VT and HT plasmas presented in this paper are in an operational domain where the average W density within the region $r/a < 0.8$ is not significantly increasing and is in fact low ($c_W \leq 3 \times 10^{-5}$) and as a result difficult to determine with the standard W analysis techniques [41].

The typical sequence of events responsible for the non-stationary plasma conditions shows the following. The central density peaking increases in time within $r/a \sim 0.5$ as shown in Figure 22 and 23 and at the same time the central temperature decreases, leading to a reduction of ST amplitude, and their eventual loss in the case of the high-δ HT plasmas, see Figs 25 and 26. The q-profile has been modified due to a change in resistivity most likely due to an increase of radiation within the

ST radius, most likely due to W. The W peaking factor can be determined with local parameter R/L_{ne}–$0.5R/L_{Te}$ as being roughly proportional to a simple analytical estimate of the neoclassical pinch to diffusivity ratio of W (RV/D) [42]. It is important to note that due to the centrifugal forces (CF) the neoclassical temperature screening is reduced and in fact the peaking factor (RV/D) is offset to higher values with a more complete calculation [43]. Figure 23 shows that as the electron density peaks, the neoclassical peaking factor RV/D reduces in amplitude and becomes even positive (leading now to a central W peaking). A more accurate calculation would show a change of sign at an earlier time in the discharge. The W concentration in the region inside the ST radius increases and the electron temperature decreases. The ST can still expelled W from the core if of high enough amplitude . Once the ST disappears a really significantly increase in W peaking factor RV/D take place increasing the W flux to the central region with no more process for expelling it. A strong central peaking of W is observed as shown from the SXR ratio accompanied with dramatic central cooling of the plasma. At this stage, the discharge is usually not recoverable and heading to a disruption [40] mitigated by the massive gas injection system either during the main plasma heating phase or during its termination [40]. The results highlight the fact that it is highly recommended to keep ST in an ELMy H-mode discharge to achieve stationarity conditions even in a case of low W contamination in the main plasma.

Such a loss of stationary plasma conditions due to density peaking is not specific to the JET- ILW and was already documented in JET-C [44, 45, 11] and many other tokamaks. The density profile is determined by the balance between outward turbulent diffusion and inward turbulent and neoclassical convection [47]. It is a well-documented effect that for plasma with density $\sim 0.8 \times n_{GW}$ or above, the neoclassical particle pinch driven by the inductive electric field (Ware pinch) is significant and that the electron density profile will be evolving towards a stationary profile determined by the peaking factor RV_{wave}/χ_{PB}, with R the major radius, V_{ware} the Ware pinch and χ_{PB} the effective heat conductivity assumed proportional to the plasma diffusivity [46]. TRANSP calculations have been done for both the high-δ HT and VT plasmas, with similar results. Here only the results for HT plasmas are reported. TRANSP calculations have shown that for shot Pulse Number: 85413, at $r/a \sim 0.4$, V_{ware} is $\sim 0.02 m.s^{-1}$ with $\chi_{PB.} \sim 0.26 m^2.s^{-1}$ corresponding to a $RV_{ware}/\chi_{PB} \sim -0.25$ and of the appropriate magnitude to be responsible for the observed increase In density [47], see Fig 24. The effect of electron density peaking due to the Ware pinch can be controlled by addition of central electron heating [48] as was done in Pulse Number: 85412 with $\sim 1 W.cm^{-3}$ .The hydrogen minority ICRH scenario in dipole strap phasing (42MHz) was used in a minority concentration X[H] of about 6%. The central heating increased the turbulent transport and therefore turbulent diffusion, χ_{PB} is raised from $\sim 0.2 m^2.s^{-1}$ to $\sim 0.5\ m^2.s^{-1}$, V_{ware} stays at the same magnitude but ratio RV_{ware}/χ_{PB} is reduced from –0.25 to –0.1 with a resulting normalised gradient length of electron density reduced at $r/a \sim 0.4$ at 13s from 1.74 to 0.6. In JET-C, a central heating of 1–2MW was sufficient to control density peaking in the HT plasmas. In JET-ILW, it is necessary to raise the RF heating to 3–5 MW, likely due to the increase radiative power from W in the plasma core, to achieve stationary plasma

conditions as shown in Figures 25 and 26. The coupling of 4–5 MW was made possible plant as well as the implementation of a technique using mid-plane localised gas injection to improve the antenna-plasma coupling. The details of this technique can be found in [49, 50, 51]. Although the Ware pinch can only play a non-negligible role on density peaking in high collisionality plasmas, it effects becomes negligible at high temperature required in a fusion reactor [47] and will not apply in ITER.

The application of RF heating in the plasma centre can control electron density peaking and as a result it is possible to achieve stationary plasma conditions. An understanding was provided for the change of the electron density peaking but not for the change in W transport. The validation of current W transport models against experimental data is an active area of research [42, 43] and has been applied on discharges Pulse Numbers: 85412 and 85413. The turbulent transport is computed with the gyrokinetic code GKW run in its local quasilinear and electrostatic limits. The neoclassical transport is computed with the local drift kinetic code NEO. In both codes, ions, electrons and impurities are all modelled kinetically, with W in the trace limits. At each radial location, the W impurity is modelled in a single average charge state Z_W between 24 (edge) and 46 (core) of the coronal equilibrium. More information on how calculations were made can be found in reference [43]. Figures 27 and 28 show the results of this GKW+NEO calculation for the diffusion and convection coefficients for W, the gradient length of W and average W profile. It indicates that the W transport is predicted to be governed by neoclassical transport from $r/a < 0.4$-0.5 and that the turbulent diffusion is dominant outside $r/a = \sim 0.5$. The calculations predict a stationary W profile that is peaking within $r/a < 0.4$ in the case without RF (Pulse Number: 85413) and hollow in the case with RF (Pulse Number: 85412). The additional temperature screening effect from the heated minority in ref [43] was also investigated but found to have a small effect compared to the difference in density peaking between these shot pairs. This means that the plasmas were made stationary possibly via three different processes, first by just counteracting the central plasma cooling with the application of heat source, second by the reduction of W source within $r/a < 0.4$ by the reduction of the density peaking and finally by the change of W transport within the plasma core as a result of the change in density gradient.

6. DEMONSTRATION OF PLASMA INTEGRATED PERFORMANCE AT JET

The avoidance of W core accumulation in high-δ N-seeded plasma with VT divertor configuration has successfully been improved by adding at least 3MW of central ICRH heating power. Long pulse operation with N-seeding was achieved in the VT configuration (less restrictive energy limit) for at least 7s (Fig29)— where the duration was limited only by the available power. It was possible to extend the plasma duration from $t_{stat}/\tau_E \sim 3$ to 28. Integrated plasma performance close to the ITER performance were achieved at JET with Be/W PFCs. These stationary ELMy H- mode plasmas are a significant step towards the ITER requirements achieving $H_{98(y,2)} \sim 0.85$, $\beta_N \sim 1.6$, $\langle n \rangle / n_{GW} \sim 0.85$, $Z_{eff} \sim 1.6$, $t_{stat}/\tau_E \sim 28$, $\Delta W_{elm}/W_{ped} \sim 4\%$ with $\Delta W_{elm} \sim 65$kJ at 45Hz ($f_{rad} \sim 0.55$) with very low

divertor target power loading and partial detachment between ELMs. Similar results have now been achieved with the JET-ILW to those previously reported with carbon PFCs using radiative ELMy H-mode scenario with N seeding [52].

7. SUMMARY AND CONCLUSION

In conclusion, progress has been made to integrate the ITER-relevant core and edge plasmas within the constraints of an ITER-like wall in JET with its Be wall and W divertor. In JET-ILW, nitrogen seeded high triangularity (high-δ) plasmas at 2.5MA achieved plasma performance of $H_{98(y,2)} \sim 0.85$, $\beta_N \sim 1.6$, $<n>/n_{GW} \sim 0.85$, $Z_{eff} \sim 1.6$ with small ELM energy losses about 65kJ corresponding to 4% of the pedestal stored energy together with partially detached divertor conditions. It was possible to maintain these plasma performances for a duration of 7s, i.e 28 times the energy confinement time, with the addition of central radio-frequency heating to control the impurity density peaking and avoid the runway effect of core W accumulation. These plasma performance are close to the desired ITER integrated plasma performance, in terms of Greenwald fraction, Z_{eff}, and divertor conditions but the normalised energy confinement needs to be increased to $H_{98(y,2)} = 1$ and the ELM energy losses need to be lowered to less than 1% of the pedestal stored energy. It remains to be proven that seeded plasma with partially detached divertor with $H_{98(y,2)} \sim 1$ and $\beta_N \sim 1.8$ are achievable at JET. This will be accessible in the next experimental campaign with higher available input power.

This paper the following was shown:

- For JET-ILW high-δ plasma with both horizontal (HT) and vertical divertor (VT) target, the strike point at the outer divertor is partially detached if the radiative power in the divertor is about 40% of the power flowing through the separatrix. This condition is also applicable in high-δ plasmas with horizontal target in JET-C with intrinsic C seeding.
- The pedestal pressure in unseeded high-δ plasmas for similar input power has decreased from JET-C to JET-ILW by 40% (for plasma with horizontal divertor geometry) and the pedestal pressure does not depend on plasma triangularity. The pedestal of the unseeded high triangularity plasmas are consistent with peeling- ballooning stability. The Peeling Ballooning (PB) stability analysis in JET-ILW requires a calculation to higher n-number than in JET-C (n = 50 instead of 30) as the pedestal is cold and has a high collisionality. The low edge current in these plasmas also provide an understanding for the lack pf dependence of the pedestal pressure on plasma triangularity, as the corner of the PB diagram cannot be accessed at high fuelling rate. However it is still not known what mechanism leads to low pedestal pressure to start with in unseeded high triangularity plasmas in JET-ILW compared to JET-C. The current idea being investigated for high triangularity plasmas is that the pedestal structure and stability are affected by a change in fuel recycling and decrease in C content. In other words, the intrinsic C seeding was playing a role in the confinement of high triangularity plasmas in JET-C that could not be studied due to the inherent presence of C.

- In JET-ILW, nitrogen seeding increases energy confinement via an increase in pedestal pressure and its effect is related to the plasma triangularity. This was observed in high triangularity plasmas both with horizontal (HT) and vertical target (VT) divertor geometry. In plasmas with vertical target divertor geometry, a 40% increase in stored energy is observed with N seeding (no JET-C reference available) with high plasma triangularity against a 15% increase for plasma with low triangularity. The mechanism that leads to an increase of pedestal pressure with nitrogen has not yet been identified but a common feature between the high-δ VT and HT plasmas is the increase of pedestal temperature.
- The dependence of ELM energy losses in N-seeded high-δ plasmas was shown to be complex and to depend on the nitrogen seeding rate, the divertor configuration, and the existence domain of type-I and type-III ELMs. It was possible to access a regime with type-III ELMs with similar plasmas performance for both high-δ HT and VT plasmas (and JET-C high-δ HT plasmas) with detached divertor conditions. At high $n_{e,ped}/n_{GW}$, the domain of existence of type-I and type-III ELMs (characterized by a critical pedestal temperature T_{crit} [9]) for 2.5MA plasmas is different if the plasma is N-seeded or unseeded. If unseeded, T_{crit} is at much lower temperature than in JET-C. With N-seeding, this critical temperature T_{crit} is lifted back to its value in JET-C for 2.5MA plasmas.
- Seeding nitrogen in the high-δ HT plasma in JET-ILW re-established the improved pedestal stability of high triangularity plasmas and the corner of the PB stability is once again accessible. Together with a wide pedestal, this leads to an increase in pedestal pressure. In contrast, the pedestal of the seeded high-δ VT plasmas has been found to be stable with respect to the PB instabilities and the increase in pedestal pressure is not due to improved pedestal stability. It is mostly due to a reduction of the ELM energy losses due to type-III ELMs together with an elevated type-I/III threshold obtained with nitrogen seeding. Further work will be needed to understand why the dependence of confinement with triangularity is then maintained.

ITER inductive scenario is designed at a triangularity $\delta \sim 0.4$ to benefit from the improved pedestal stability of high triangularity plasma. It is still unclear if the ITER pedestal will be unstable with respect to the peeling instabilities or the ballooning instabilities, i.e. in a similar region of the PB diagram as JET is. Experiments on JET need to be conducted to explore the effect of impurity seeding on the pedestal stability and confinement for plasmas that are peeling rather than ballooning limited to broaden the understanding and to expand the extrapolability of the impact of seeding on pedestal confinement towards future fusion devices for low collissionality plasmas. Our understanding of the confinement of high triangularity plasmas has been challenged by the unexpected decrease in pedestal pressure with a change of plasma facing components and the identification of the mechanism at play has to be an area of active research.

ACKNOWLEDGEMENTS

This work was carried out within the framework of the European Fusion Development Agreement. For further information on the contents of this paper please contact publications- officer@jet.efda.org. The views and opinions expressed herein do not necessarily reflect those of the European Commission. This work was also part-funded by the RCUK Energy Programme under grant EP/I501045

REFERENCES

[1]. Doyle et al, Nuclear Fusion **47** (2007) S18–S127 doi:10.1088/0029-5515/47/6/S02
[2]. H. Zohm et al, Nuclear Fusion **53** (2013) 073019
[3]. A. Loarte et al , Physics of Plasmas **18**, 056105 (2011)
[4]. R.A Pitts at al, Journal of Nuclear Materials **438** (2013) S48-S56 http://dx.doi.org/10.1016/j.jnucmat.2013.01.008
[5]. Scarabosio A. submitted to Journal of Nuclear Materials
[6]. A. S. Kukushkin et al, Nuclear Fusion **49**, 075008 (2009).
[7]. A. Loarte et al, Nuclear Fusion **54** (2014) 033007 http://dx.doi.org/10.1088/0029-5515/54/3/033007
[8]. Hawryluk R.J. et al, Nuclear Fusion **49** (2009) 065012 http://dx.doi.org/10.1088/0029-5515/49/6/065012
[9]. Sartori R. et al, Plasma Physics and Controlled Fusion **46** (2004) 723–750
[10]. Campbell D J et al, 2001 Physics of Plasmas **8** 2041
[11]. Saibene G. et al 2002 Plasma Physics and Controlled Fusion **44** 1769–99
[12]. Giroud C. et al 2012 Nuclear Fusion **52** 063022
[13]. Giroud C. et al, Nuclear Fusion **53** (2013) 113025
[14]. Stober J et al 2000 Plasma Physics and Controlled Fusion **42** A211–6
[15]. H. Urano et al 2002 Plasma Physics and Controlled Fusion **44** 11
[16]. T.H. Osborne et al 2000 Plasma Physics and Controlled Fusion **42** A175
[17]. D. Moulton et al 2011, Journal of Nuclear Materials **415** S509–12
[18]. Brezinsek S. et al 2013 Journal of Nuclear Materials **438** S303–8
[19]. G.P. Maddison et al Nuclear Fusion **54** (2014) 073016 http://dx.doi.org/10.1088/0029-5515/54/7/073016
[20]. Jarvinen A et al, submitted to Journal of Nuclear Materials.
[21]. L. Frassinetti et al, submitted to Nuclear Fusion
[22]. B. Sieglin et al, Plasma Physics and Controlled Fusion **55** (2013) 124039 http://dx.doi.org/10.1088/0741-3335/55/12/124039
[23]. Matthews 2013
[24]. Schweinzer J. et al 2011 Nuclear Fusion **51** 113003
[25]. Tardini G et al 2013 Plasma Physics and Controlled Fusion **55** 015010
[26]. Joffrin E, EPS Berlin 2014.
[27]. Jarvinen A et al, IAEA 2014

[28]. Beurskens M. et al, Plasma Physics and Controlled Fusion, **55**,(2013) 124043
[29]. Maddison G. et al 2010 Journal of Nuclear Materials **415** S313–7
[30]. Maddison G. et al, 2011 Nuclear Fusion **51** 042001
[31]. Mikhailovskii A.B. et al 1997 Plasma Physics Reports **23** 844
[32]. Snyder P.B. et al Physics of Plasmas **95**
[33]. Wilson H.R. et al Physics of Plasmas **94**
[34]. Saarelma S. et al 2009 Plasma Physics and Controlled Fusion 51 035001
[35]. Sauter O. and Angloni C. 1999 Physics of Plasmas **6** 2834–9
[36]. Neu R.et al. Journal of Nuclear Materials **438** (2013) S34–S41
[37]. Snyder P.B. et al Nuclear Fusion **51** (2011) 103016
[38]. Maget P. et al, Nuclear Fusion **53** (2013) 093011
[39]. Saarelma S. et al., Nuclear Fusion **52** (2012) 103020
[40]. de Vries P. et al Plasma Physics and Controlled Fusion **54** (2012) 124032
[41]. Puetterich T. et al, Plasma Physics and Controlled Fusion **55** (2013) 124036
[42]. C. Angioni et al., Nuclear Fusion (in Press) (2014)
[43]. http://arxiv.org/abs/1407.1191
[44]. M. Valovic et al Plasma Physics and Controlled Fusion **44** (2002)
[45]. Nave M.F.F. et al 2003 Nuclear Fusion **43** 1204–13
[46]. Stober J et al, Plasma Physics and Controlled Fusion **43** (2001) A39–A53
[47]. Angioni C. Et al, Plasma Physics and Controlled Fusion **51** (2009) 124017
[48]. Rice, J.E. et al, Nuclear Fusion **42** (2002) 510–519
[49]. Lerche E. et al, Journal of Nuclear Materials 2014.
[50]. Jacquet P. Et al, IAEA 2014
[51]. Goniche M et al, EPS Berlin 2014.
[52]. Rapp J et al, Nuclear Fusion **49** (2009) 095012

	high-δ HT JET-C	high-δ HT JET-ILW	high-δ VT JET-ILW	low-δ HT JET-ILW	low-δ VT JET-ILW
Ip/Bt	2.5MA/2.7T	2.5MA/2.7T	2.5MA/2.7T	2.5MA/2.7T	2.5MA/2.8T
q95	3.5	3.4	3.2	3.4	3.4
Upper/lower δ	0.44/0.39	0.37/0.37	0.40/0.34	0.35/0.19	0.26/0.18
Plasma vol.(m^{-3})	74	74	72	75	76
P_{NBI}/P_{RF} (MW)	14-15/ 1.5	14-18/0-4	15-17/0-4	15-20/0	16/0
D_2 Γ_{el} (10^{22}el/s)	0.22-6.0	0.7-4.5	0.9-2.9	0.8-2.7	2.8
N_2 Γ_{el} (10^{22}el/s)	0-4.5	0-3.6	0-3.4	0-2.5	2.18

Table 1: Summary of key parameters for plasma scenario of all JET pulses considered in this paper.

pulse	config	Γ_D (10^{22} el/s)	Γ_N (10^{22} el/s)	H_{98}	$n_{e,ped}/n_{GW}$	βn	Z_{eff}	ΔW_{elm} (kJ)	f_{elm} (Hz)	$\Delta W_{elm}/W_{ped}$ (%)
76666	HT	0.37	0	0.97	0.66	1.85	1.93	160	20	9
76678	HT	2.71	0	0.95	0.9	1.9	1.7	200	8	10
76687	HT	1.83	4.45	0.86	0.68	1.54	2.26	20	70	1
76681	HT	2.69	4.40	0.78	0.67	1.34	2.17	30	52	2
82806	HT	2.89	0	0.7	0.76	1.1	1.25	90	16	8
82810	HT	2.67	2.61	0.84	0.94	1.65	1.31	130	16	7
82812	HT	2.69	2.44	0.85	0.90	1.78	1.53	154	20	10
82819*	HT	0.84	2.53	0.87	0.70	1.60	1.65	64	35	5
82817	HT	1.49	2.93	0.90	0.85	1.82	1.43	153	20	9
85413	HT	2.74	3.46	0.81	0.80	1.70	1.54	100	32	6
85414	HT	2.76	3.56	0.85	0.81	1.93	1.56	80	40	4
82811	HT	2.84	3.61	0.80	0.81	1.50	1.72	70	40	5
85412	HT	2.61	3.46	0.86	0.76	1.6	1.9	66	48	5
85262	VT	2.71	0	0.61	0.70	1.06	1.28	95	13	10
85263	VT	2.11	0	0.60	0.72	1.03	1.26	100	14	10
85266	VT	2.10	1.79	0.83	0.63	1.53	1.63	54	50	4
85270	VT	2.13	3.0	0.85	0.63	1.61	1.60	57	53	3
85419	VT	2.9	2.6	0.85	0.64	1.6	1.4	65	45	5

*Table 2: Summary of performance and ELM energy losses of high-δ plasmas in this study: Here are shown the configuration type, the fuelling and N-seeding rate, normalized confinement, ratio of $n_{e,ped}$ over n_{GW}, normalized pressure, Z_{eff} measured by bremstrahlung, ELM energy losses, ELM frequency, and ratio of ELM energy losses over the stored pedestal energy. Pulse with * correspond to a data point that could not be reproduced on another experimental day. All pulse below 80000 shown in this Table are from JET-C, the others are from JET-ILW.*

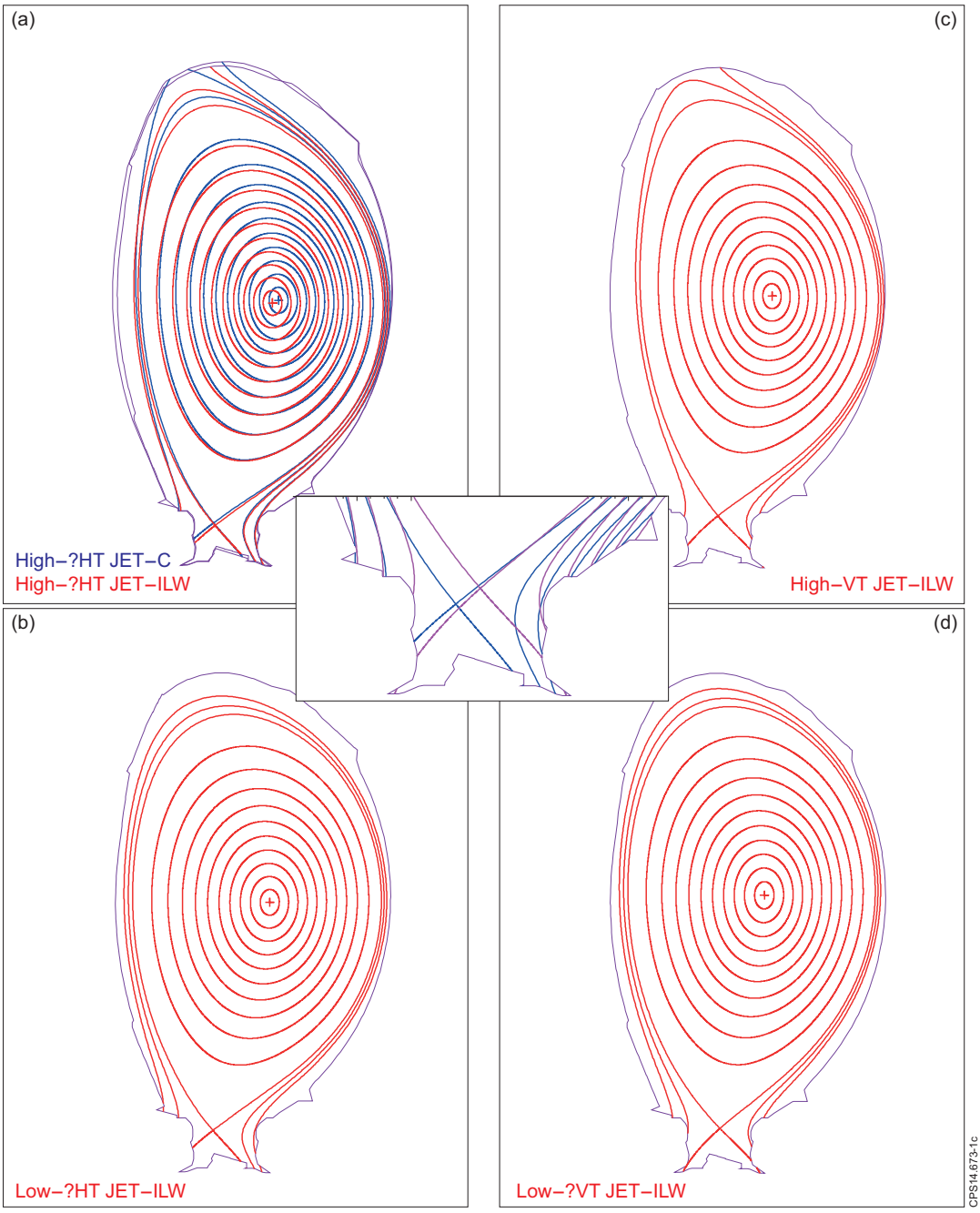

Figure 1: Configuration of the five plasma configuration used in this study (a): the high-δ horizontal divertor target (HT) plasmas in JET-C in blue (Pulse Number: 76666 at 20s) and JET-ILW in red, (Pulse Number: 82806 at 15s); (b) the low-δ HT (Pulse Number: 83177 at 15s); (c) the high-δ vertical divertor target (VT) plasmas with both inner and outer strike on vertical divertor plates (85267 at 15s); (c) the low-δ VT plasmas (Pulse Number: 83487 at 15s). The inset illustrates the difference in divertor configuration between the HT (blue) and VT plasmas (in red). Configurations in red were used in JET-ILW and in blue in JET-C.

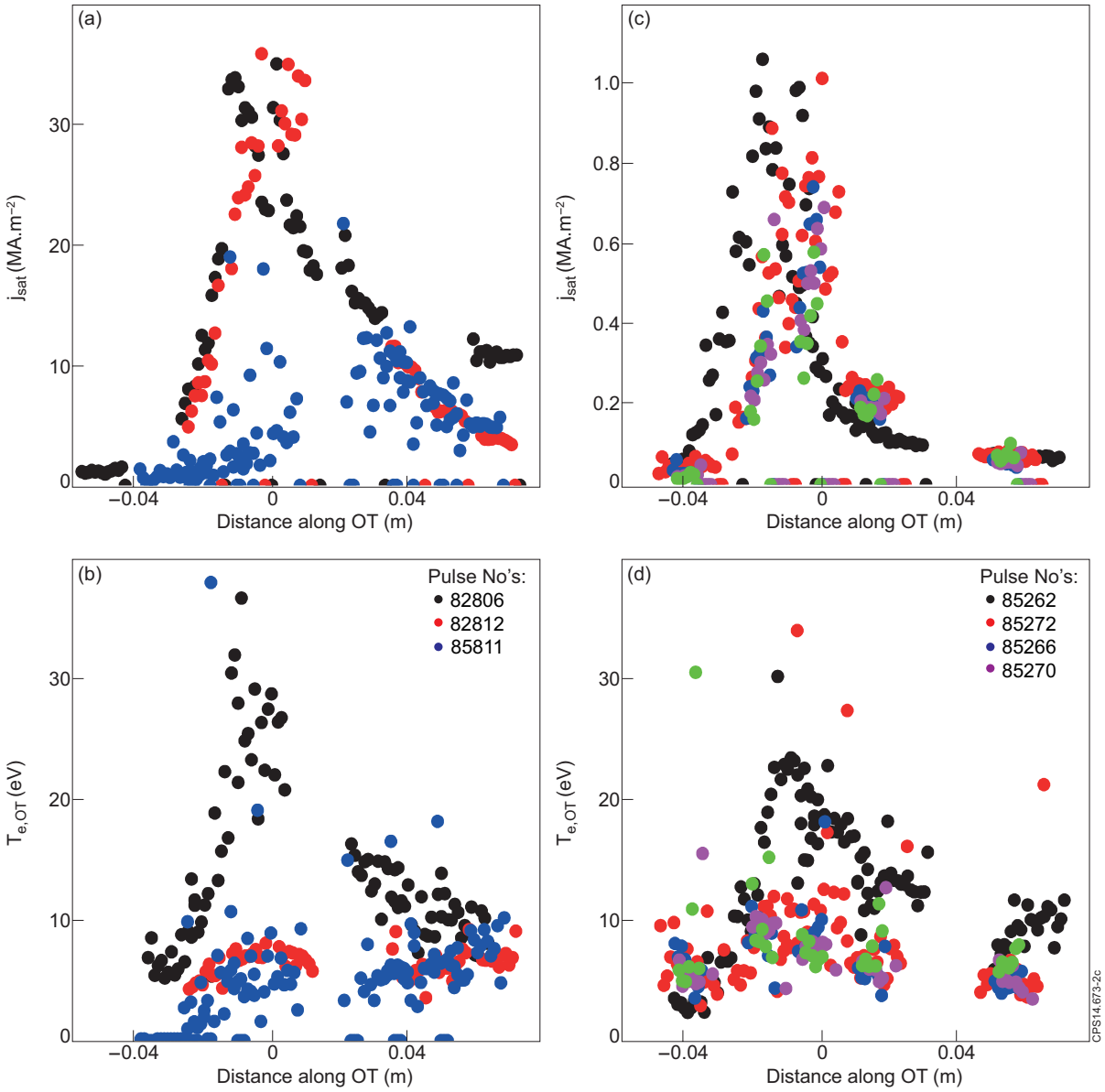

Figure 2: JET-ILW Ion saturation current profiles (I_{sat} in MA.m^{-2}) and electron temperature profiles (Te_{OT} in eV)at outer divertor target measured by Langmuir probes (LP: a) and b) are the I_{sat} and Te_{OT} profiles for high-δ HT plasmas at different N-seeding rate ($\Gamma_N \sim 0 \times 10^{22}$ el/s (Pulse Number: 82806), $\Gamma_N \sim 2.4 \times 10^{22}$ el/s (Pulse Number: 82812) and $\Gamma_N \sim 3.6 \times 10^{22}$ el/s(Pulse Number: 82811), and at the fuelling rate of 2.8×10^{22} el/s. c) and d) are the I_{sat} and Te_{OT} profiles for high-δ VT plasmas at the fuelling rate of 2×10^{22} el/s and at increasing N-seeding rate ($\Gamma_N \sim 0$ (Pulse Number: 85262), $\Gamma_N \sim 1.2$ (Pulse Number: 85272) and $\Gamma_N \sim 1.8$ (Pulse Number: 85266) and $\Gamma_N \sim 3.\times 10^{22}$ el/s(Pulse Number: 85270).

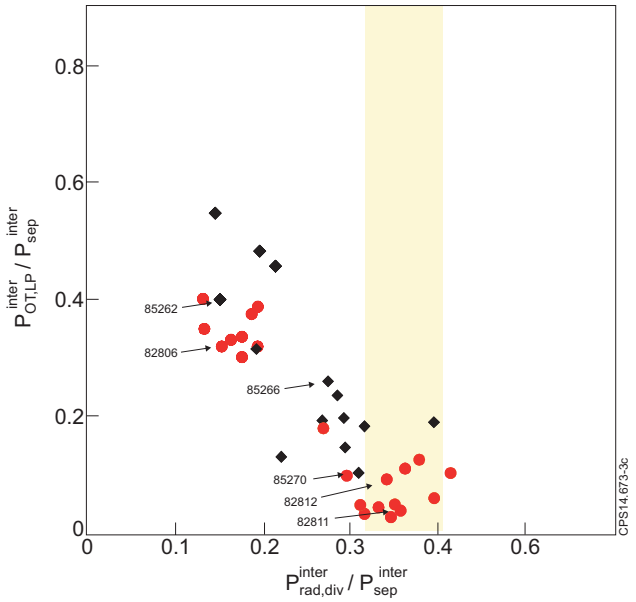

Figure 3: Ratio of power reaching the OT measured with LP to power flowing through the separatrix (P_{sep}) versus ratio of divertor radiation to Psep in the inter-ELM period for JET- for two divertor configurations: high-δ HT (red circles) and VT plasmas (black diamonds).

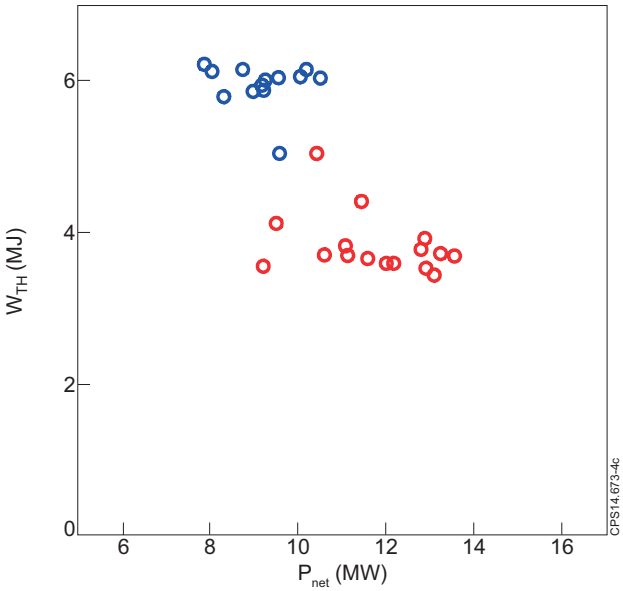

Fig 4: Stored energy versus Pnet in unseeded high-δ HT plasma in JET-C and JET-ILW, in blue and red respectively. Pnet is the input power Pin minus the radiative power in the main plasmas, $P_{rad,main}$.

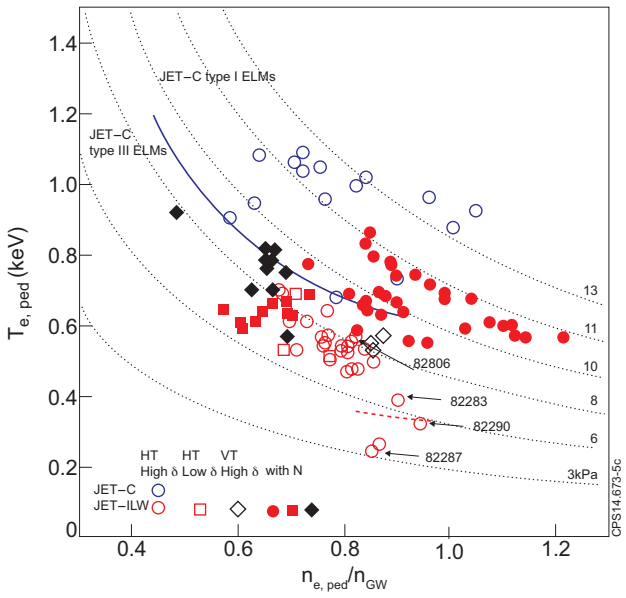

Figure 5: Pre-ELM pedestal temperature versus pedestal density for JET-C (Blue symbols) and JET-ILW: red circles for high-δ HT plasmas; black diamonds for high-δ VT plasmas; and red squares for low-δ HT plasmas. The blue line indicated the experimentally observed threshold for the transition from Type I to Type III ELM regime in JET-C. [13] The red dashed line indicate where the area where transition from Type-I to Type-III ELM regime is in JET-ILW.

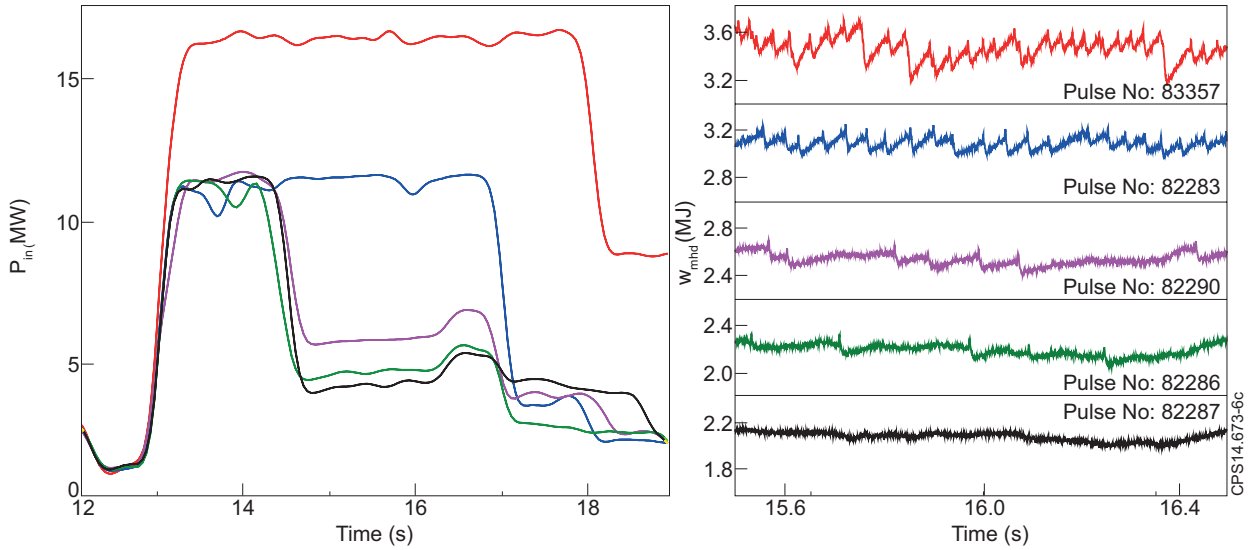

Figure 6: Power ramp-down in main heating phase for determination of back-transition from type-I to type-III ELM regime: (left to right) total heating power and stored energy versus time for unseeded discharges at fuelling rate of 3–4 × 10^{22} el/s.

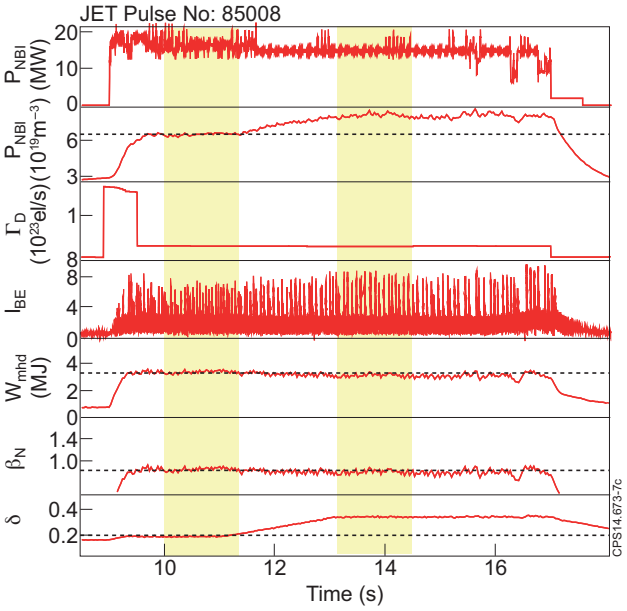

Figure 7: Dependence of stored energy with triangularity in unseeded plasmas: highlighted region show the time window for low-δ VT (δ = 0.22) and high-δ VT plasmas (δ = 0.37).

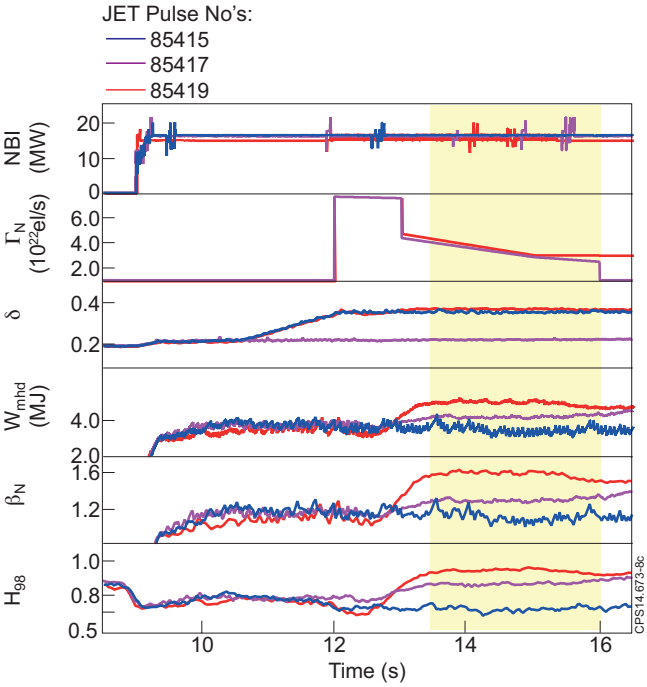

Figure 8: Dependence of stored energy with plasma triangularity and N-seeding: (from top to bottom) neutral beam heating, ion cyclotron heating power, fuelling and N-seeding rate, stored energy, normalized pressure, $H_{98(Y,2)}$ and triangularity for pulse numbers 85415 (blue), 85417 (pink) and 85419 (red).

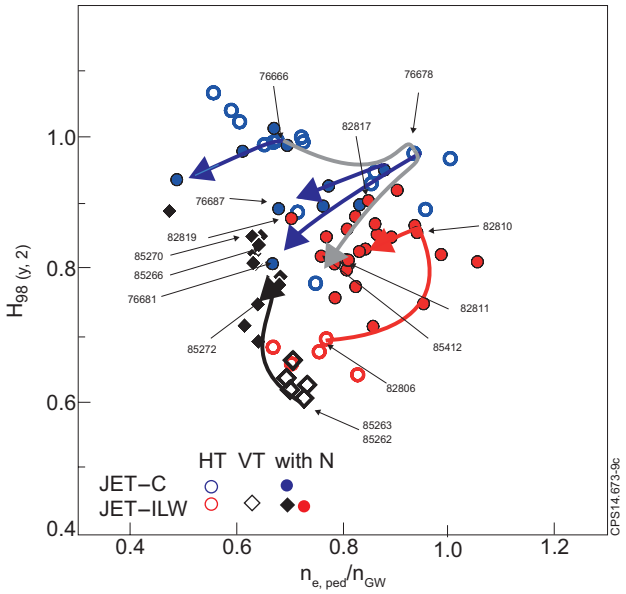

Figure 9: $H_{98(y,2)}$ versus ratio of ELM-averaged electron pedestal density over Greenwald density for high-δ plasmas ($f_G = n_{e,ped}/n_{GW}$). The lines and arrow indicate respectively in grey increase of D-fuelling in successive discharges in JET-C. The impact of N-seeding is indicated for JET-C in blue and leads to modest reduction in $H_{98(y,2)}$ For JET-ILW in red (HT) and black(VT), N_2 seeding leads to a significant improvement in $H_{98(y,2)}$. The different Greenwald density fraction f_G between high-δ HT and VT is thought to be due to a different plasma cross-section.

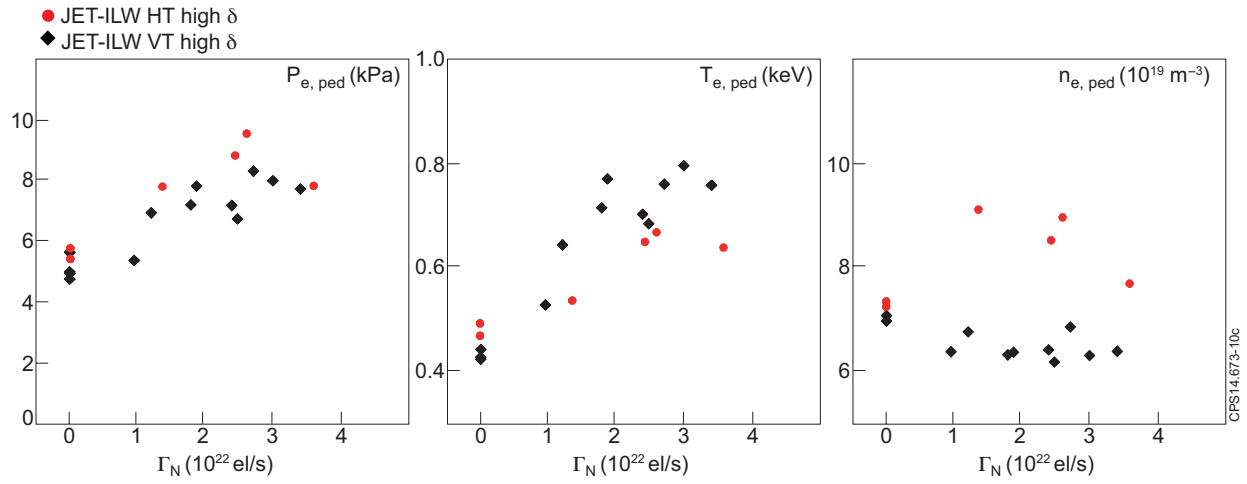

Figure 10: ELM-average pedestal electron temperature, density and pressure versus nitrogen seeding rate in high-δ HT and VT plasmas. Red circles correspond to high-δ HT plasmas. Black diamonds correspond to high-δ VT plasmas. N-seeded discharges are in filled symbols. Unseeded discharge in open symbols.

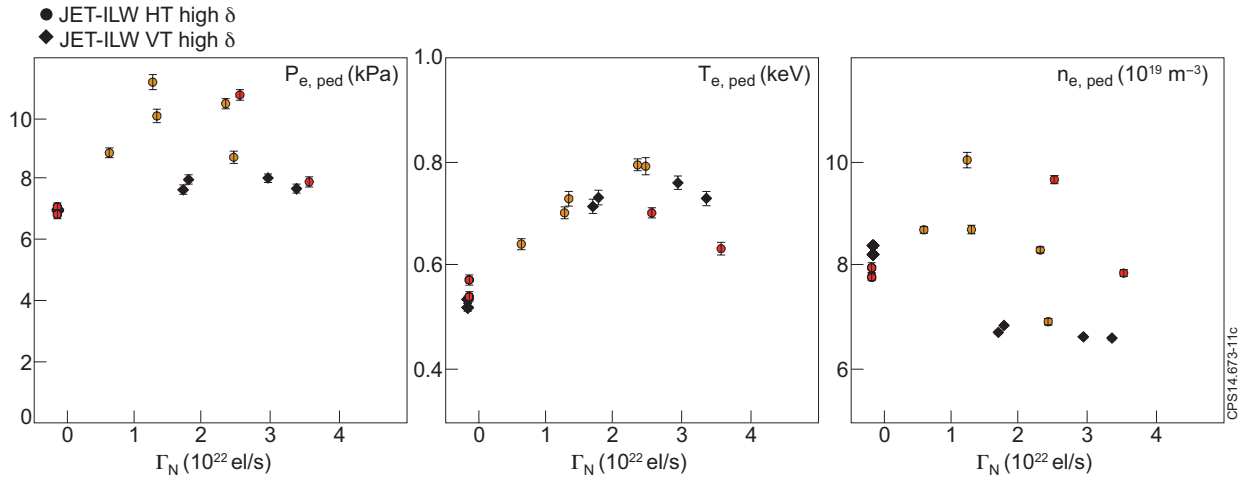

Figure 11: Pre-ELM pedestal pressure, temperature and density height in the time period 70 to 90% before an ELM as a function of the nitrogen seeding rate: Black diamond correspond to high-δ VT plasmas. Circles correspond to high-δ HT plasmas, red and yellow for fuelling rate greater and lower than 2×10^{22} el/s, respectively.

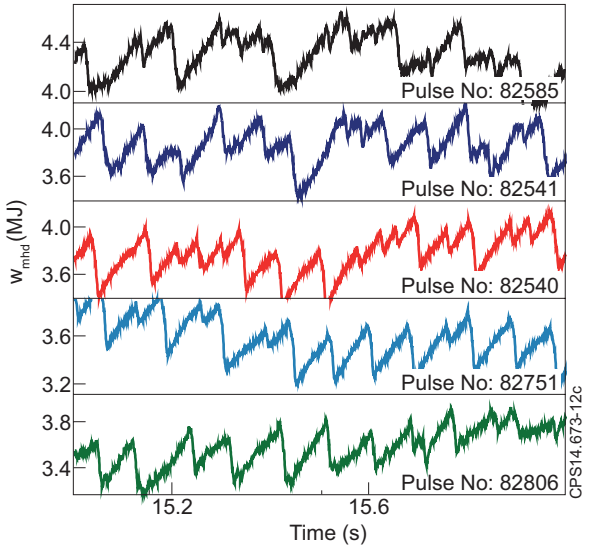

Figure 12: Stored energy versus time of JET-ILW high-δ HT unseeded discharges, with for Pulse Numbers: 82585, 82541, 82540, 82751,82806 a D-fuelling rate of 0.9, 1.5,1.8,3., 2.89, 4.4 × 10^{22} el/s respectively.

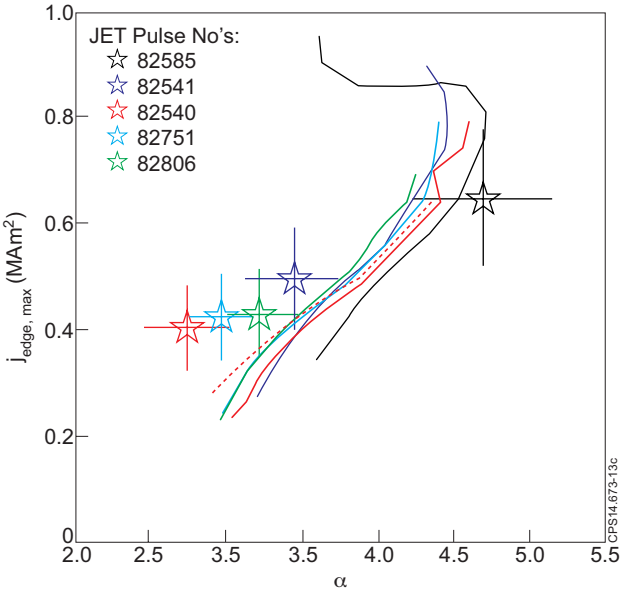

Figure 13: PB stability analysis for fuelling scan in JET-ILW high-δ HT plasma. The dashed line represents n < 70. The solid lines are calculated using n < 50.

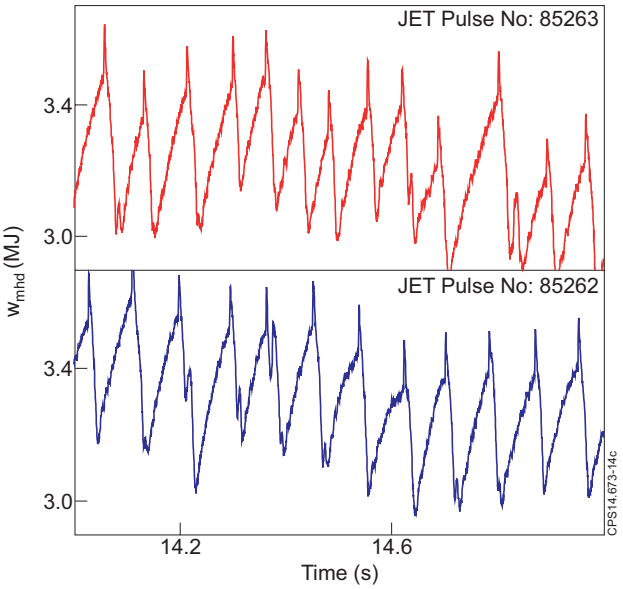

Figure 14: Stored energy versus time of unseeded high-δ VT plasmas. Stored energy versus time of JET-ILW high-δ VT unseeded discharges, with a fuelling rate of 2×10^{22} el/s respectively.

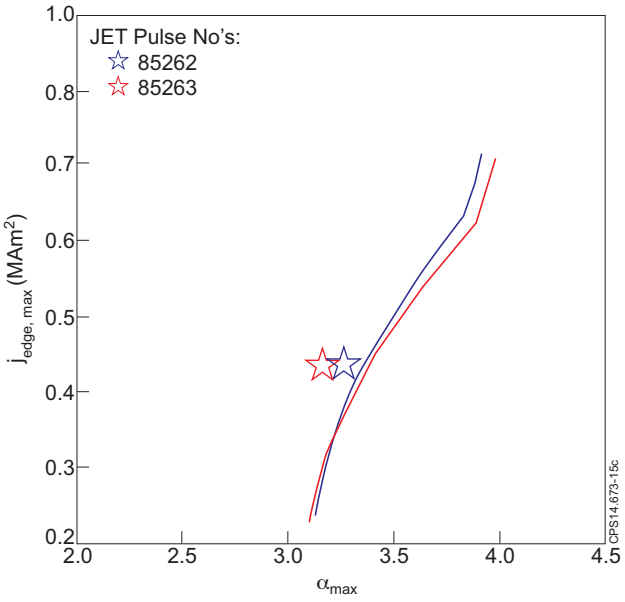

Figure 15: PB stability analysis for fuelling scan in JET-ILW high-δ VT plasma. The solid lines are calculated using $n < 50$.

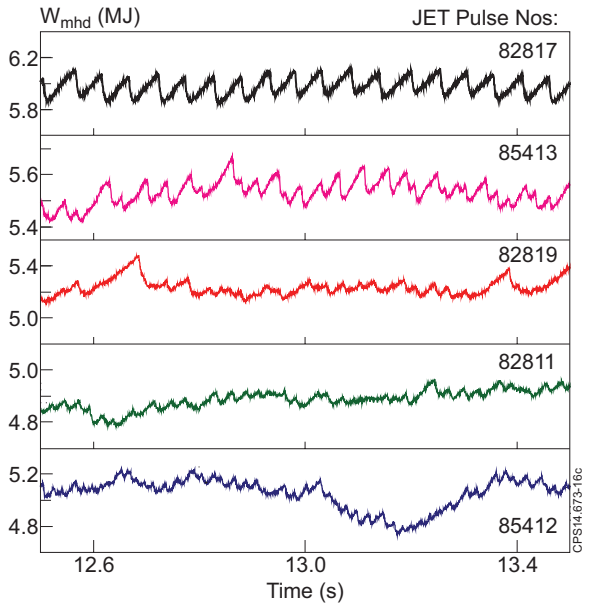

Figure 16: Stored energy versus time of JET-ILW high-δ HT N-seeded discharges in JET-ILW, with for Pulse Numbers: 82817 (2.7/3.4), 85413 (2.5/3.0), 82819 (2.9/3.6), 82811 (0.8/2.5), 85412 (2.6/3.4) with D-fuelling/N- seeding rate between parenthesis in unit 10^{22} el/s. Time traces for Pulse Numbers: 85412 and 85413 have been delayed by 3s for display purpose.

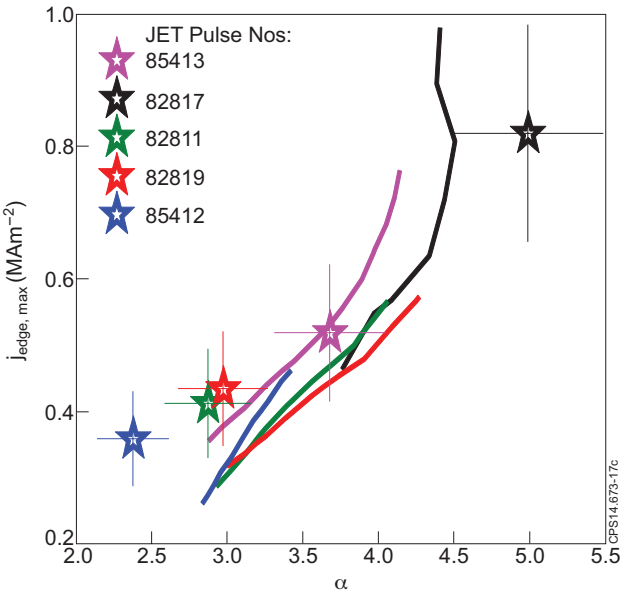

Figure 17: PB stability analysis for N-seeded high-δ HT plasmas in JET-ILW. For all pulses the PB stability is calculated up to n = 50.

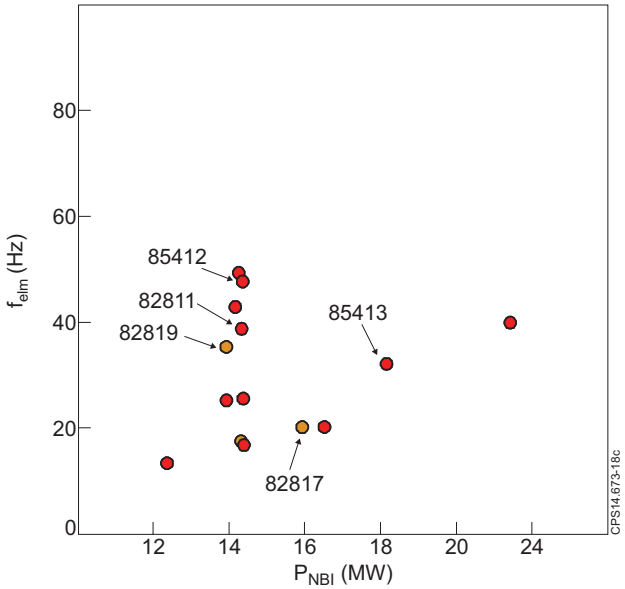

Figure 18: ELM frequency versus neutral beam power for high-δ HT plasma with N-seeding rate above 2×10^{22} el/s and fuelling above 0.8×10^{22} el/s

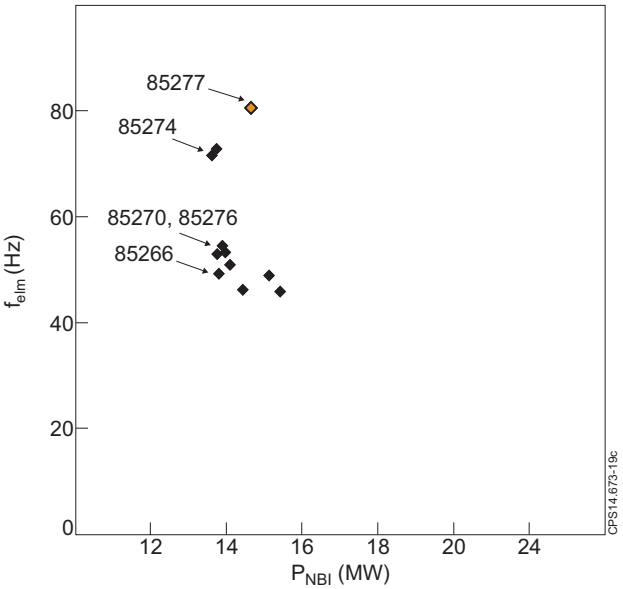

Figure 19: ELM frequency versus neutral beam power for high-δ VT plasma with N-seeding rate above 1.5×10^{22} el/s and fuelling above 0.8×10^{22} el/s

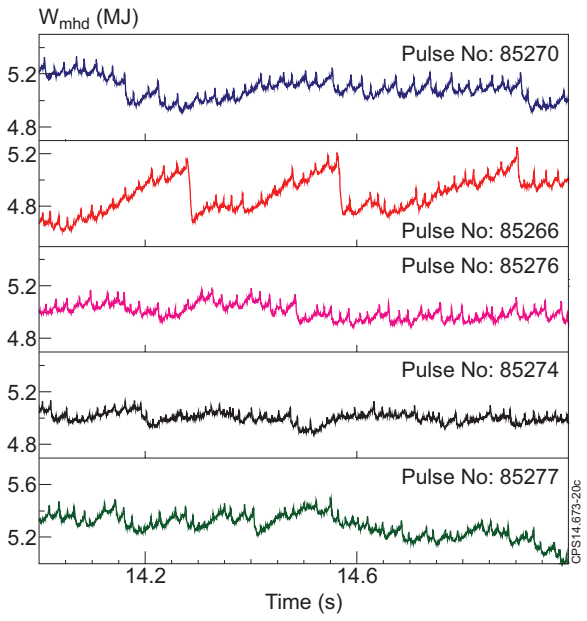

Figure 20: Stored energy versus time of N-seeded high-δ VT plasmas

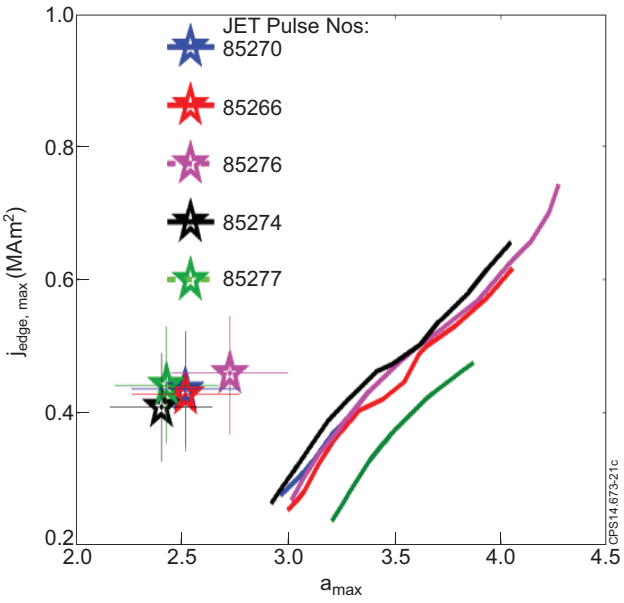

Figure 21: PB stability analysis for N-seeded high-δ VT plasmas in JET-ILW. For all pulses the PB stability is calculated up to n = 50.

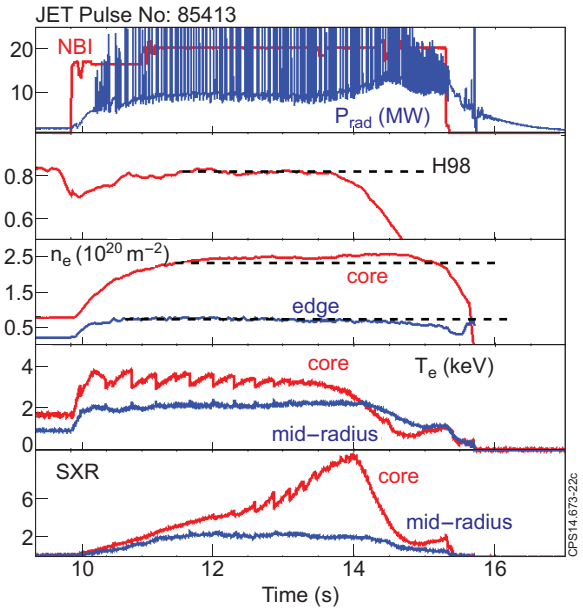

Figure 22: Time trace of N-seeded high-δ HT plasmas discharge Pulse Number: 85413, (from top to bottom) NBI heating and total radiated power, normalised energy confinement factor $H_{98(y,2)}$ core and edge density measured by interferometry, electron temperature measured with ECE in the core and at mid-radius, and soft x-ray radiated power measured from the channel crossing the core plasma and one at mid-radius. Mitigated disruption occurs at 15.64s.

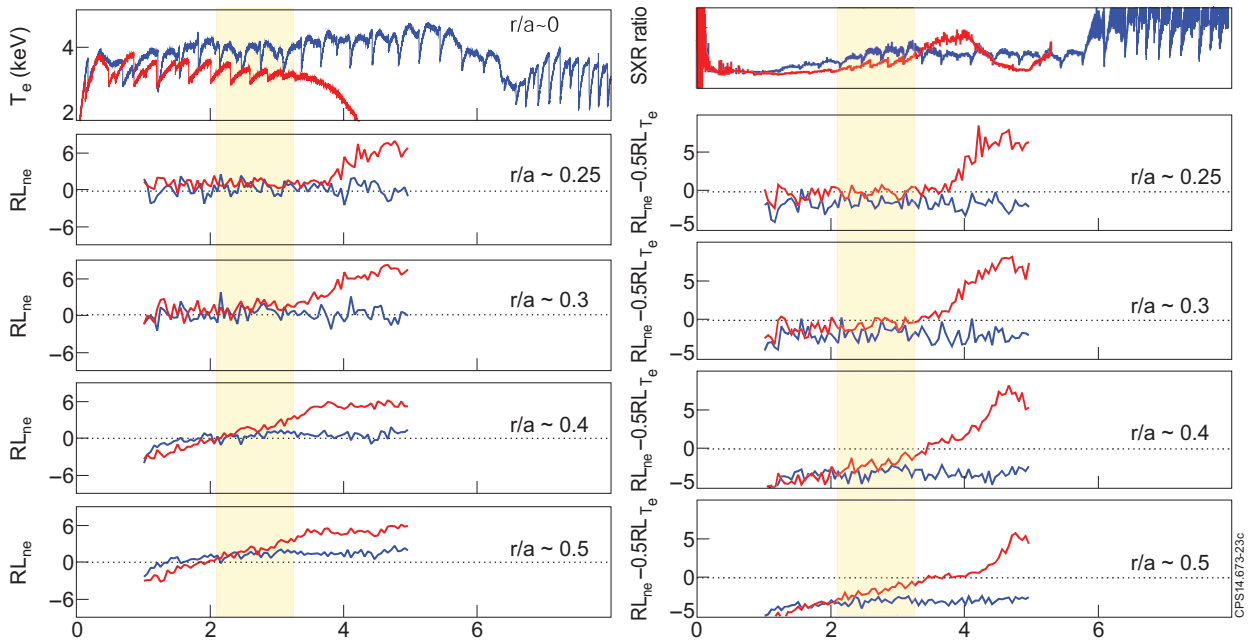

Figure 23: Evolution in time of central core temperature measured with ECE, electron density gradient length measured at various r/a, ratio of SXR signal of line-of-sight going through the plasma core at mid-radius., R/Lne-0.5R/LTe at various central r/a, for Pulse Number: 85413 in red and 85412 in blue. X-axis t = 0 is the time of start of NBI heating.

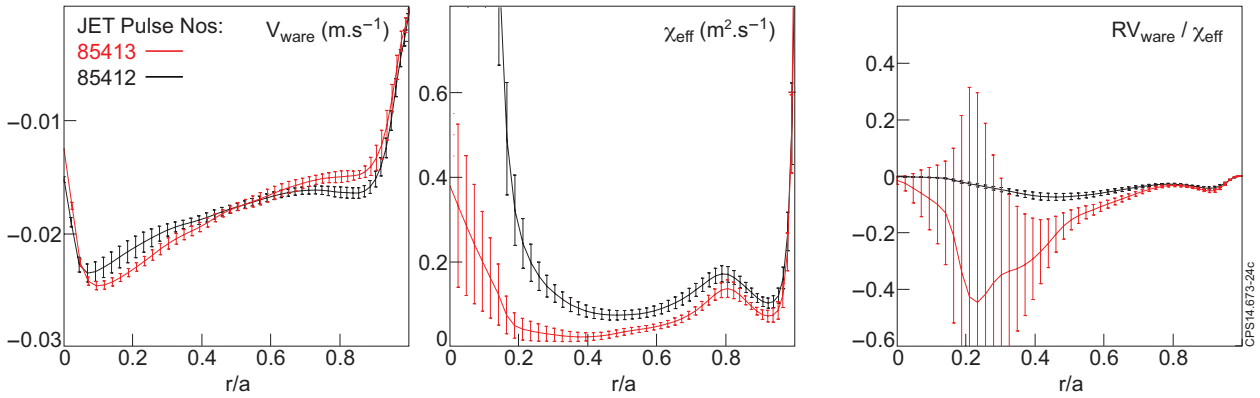

Figure 24: Ware pinch, effective heat conductivity χ_{PB} and peaking factor RV_{wave}/χ_{PB} calculated with TRANSP for Pulse Number: 85412 (black, with RF) and Pulse Number: 85413 (red, w/o RF) time-average between 12.5 and 13.5s

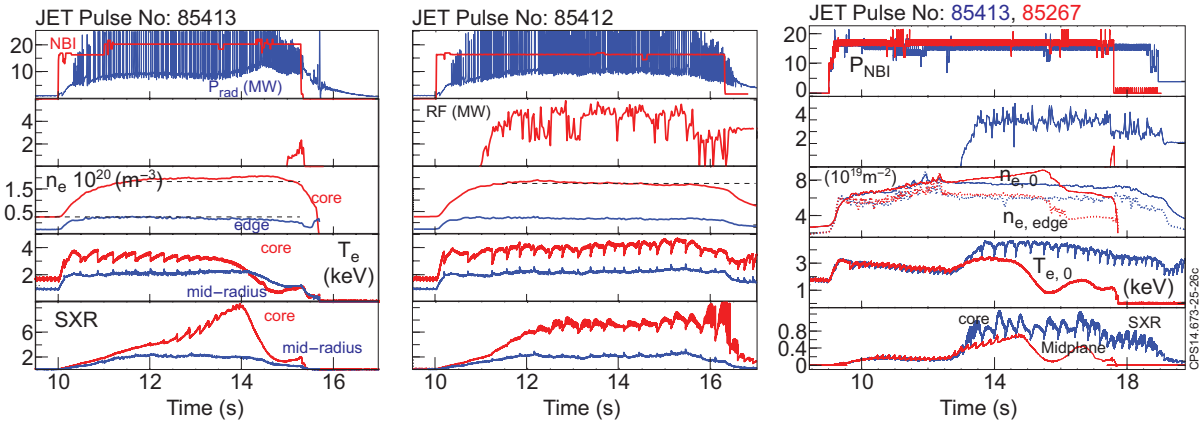

Figure 25: Time trace of N-seeded high-δ HT plasmas discharge Pulse Number's: 85413 and 85412, (from top to bottom) NBI heating and total radiated power, Rf heating power, core and edge density measured by interferometry, electron temperature measured with ECE in the core and at mid-radius, and soft x-ray radiated power measured from the channel crossing the core plasma and one at mid-radius.

Figure 26: Time trace of N-seeded high-δ VT plasmas discharge Pulse Number's: 85266 and 85267 (from top to bottom) same as figure 25.

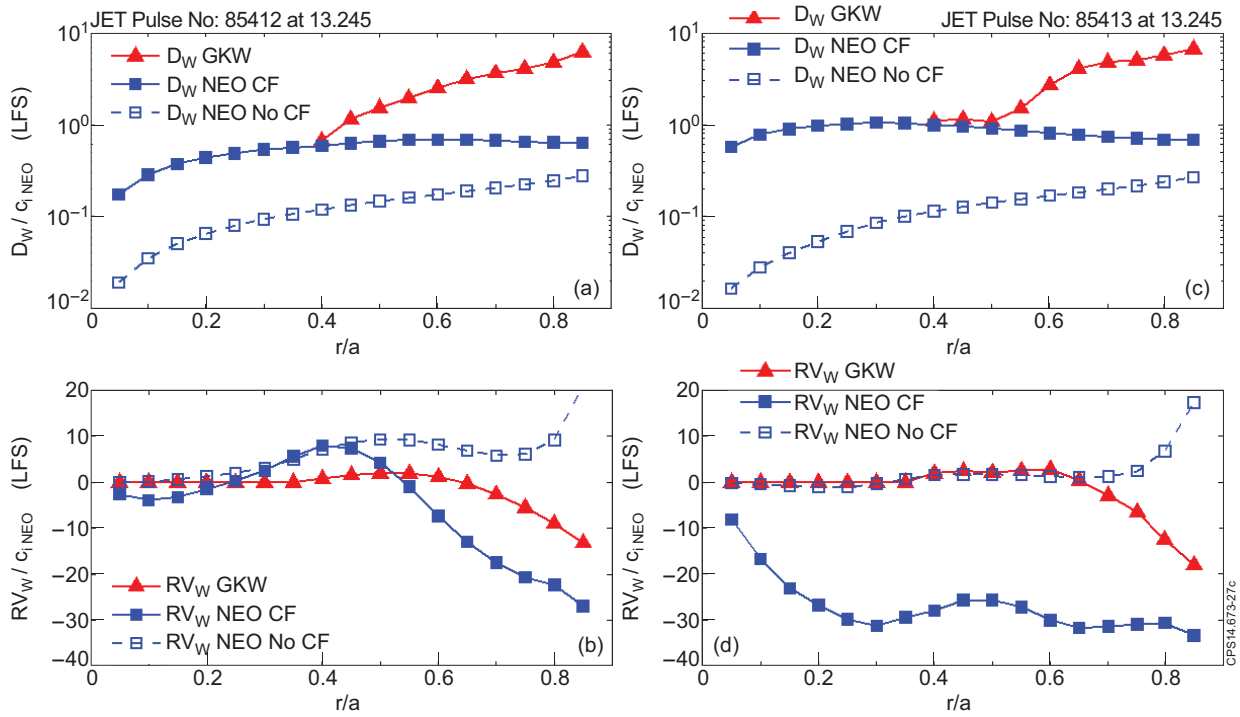

Figure 27: Predicted W transport coefficients (LFS) calculated with GKW+NEO (GKW) for Pulse Number's: 85412 and 85413 between 13.2s and 13.3s, with additional simulations with only NEO with (CF) and without centrifugal force (no CF).

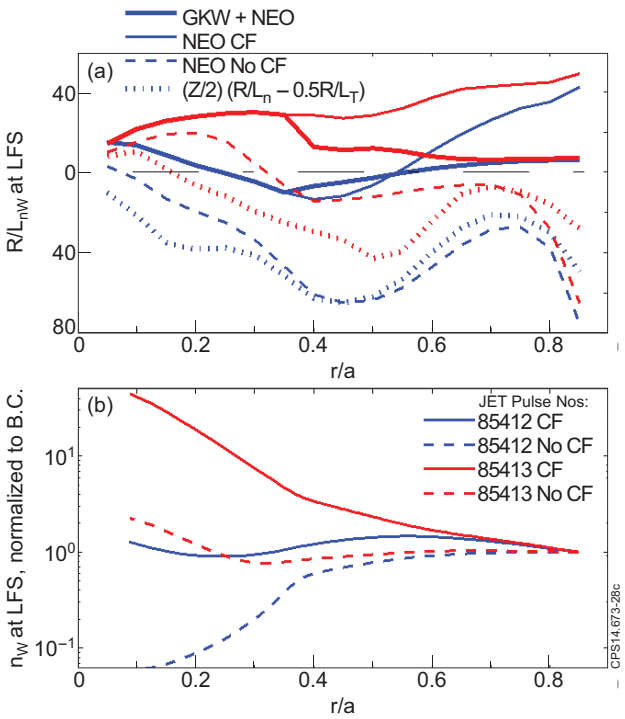

Figure 28: Predicted R/L_{nw} and integrated nw profiles from Pulse Numbers: 85413 and 85412.13.2 and 13.3s. Predicted W transport coefficients (LFS) calculated with GKW+NEO (GKW+NEO) for Pulse Numbers: 85412 and 85413 between 13.2s and 13.3 s, with additional simulations with only NEO with (CF) and without centrifugal force (no CF). A simple analytical estimate of neoclassical peaking (dots) closely follows the neoclassical results without CF effects.

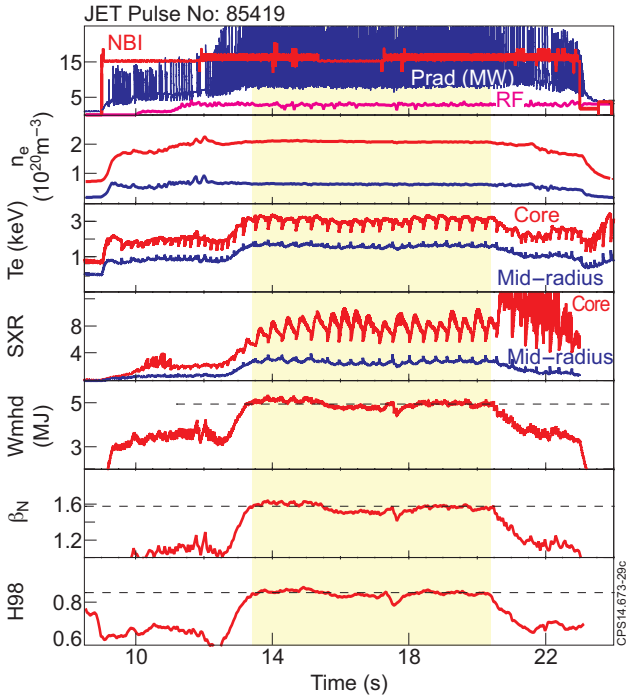

Figure 29: Time-trace for long N_2-seeded Pulse Number: 85419 at 2.5MA/2.7T (VT).